Immune control of tumor stemness and therapy resistance

Francesca Maria Consonni[*1,2], Anna Pastò[*1,5], Giulia Ballerini[*1,2], Mariangela Storto[1,6], Francesca Guana[3], Martina Incerti[1,2], Marina Sironi[1], Paola Ostano[3], Giovanna Chiorino[3], Alberto Amadori[4], Antonio Sica[1,2]

[1]IRCCS Humanitas Research Hospital, Rozzano, Milan, Italy; [2]Department of Pharmaceutical Sciences, University of Piemonte Orientale "A. Avogadro", Novara, Italy; [3]Genomics Lab, Fondazione "Edo ed Elvo Tempia", Biella, Italy; [4]Immunology and Molecular Oncology Unit, Veneto Institute of Oncology IOV-IRCCS, 35128 Padova, Italy. [5] Current address Oncology Translational Research, GlaxoSmithKline, Stevenage SG12NY, United Kingdom. [6]Current address: San Raffaele-Telethon Institute for Gene Therapy (SR-TIGET), IRCCS San Raffaele Scientific Institute, Milan, Italy.

[*]The first three authors contributed equally to this study

Corresponding author: Antonio Sica; Phone: +39.02.8224.5111; Fax:+39.02.8224.5101; Email: antonio.sica@uniupo.it; antonio.sica@humanitasresearch.it

Running title: Immunomodulation of cancer stemness

Funding Information:

This work was supported by Associazione Italiana per la Ricerca sul Cancro (AIRC) IG (No. 29348 to AS); AIRC 5x1000 (no. 22757 to AS); Ministero Università Ricerca (PRIN 20227YR8AW to AS; PRIN 2022T3ZALK to FMC); Associazione "Augusto per la Vita" Novellara (RE), Italy; Fondazione "Aiace", Bologna, Italy; Associazione "Medicine Rocks", Milano, Italy; Fondazione Giancarlo Ligabue (Venezia), Italy,

Downloaded from aacrjournals.org/cancerimmunolres/article-pdf/doi/10.1158/2326-6066.CIR-26-0211/3849116/cir-26-0211.pdf by guest on 22 November 2026

ABSTRACT

Cancer stem cells (CSC) are a small group of tumor cells capable of self-renewing, giving rise to new tumors, and resisting treatment, thereby causing recurrence and metastasis and representing a serious clinical problem. However, there are no approved therapies for their elimination, and limited information is available on the effects of current therapies on tumor stemness. A general consensus suggests that the anti-inflammatory and immunosuppressive tumor microenvironment promotes tumor stemness. Since we previously reported that ablation of the p50 NF-κB gene in the hematopoietic compartment ($p50^{fl/fl}$*Tie2-Cre* mice) restores M1/Th1 antitumor immunity, we studied its effects on CSC and therapy resistance in models of fibrosarcoma and melanoma. Using $p50^{fl/fl}$*Tie2-Cre* mice, we demonstrate that p50 NF-κB silencing impairs CSC development, their migratory capacity, and epithelial-mesenchymal transition (EMT), events known to correlate with tumor aggressiveness. Furthermore, we identify a clear antagonistic effect between Th1 and Th2 T cell polarization, with the former acting as inhibitors and the latter promoting the stemness phenotype. Consistently, while immunotherapy with anti-PD-1 promoted a marked reduction in CSC and tumor development, associated with increased levels of IFNγ, whereas concomitant administration of anti-IFNγ antibodies restored tumor growth and dissemination. Moreover, treatment with anti-IL-4 enhanced the antitumor effects of immunotherapy, reducing tumor cell stemness. Importantly, the antitumor effects of high-dose IFNγ and anti-IL-4 were confirmed in combination with doxorubicin chemotherapy. Overall, our data indicate that shifting the immune response toward a robust M1/Th1 state can significantly improve current immunotherapies and chemotherapies, by limiting CSC properties.

Downloaded from aacrjournals.org/cancerimmunolres/article-pdf/doi/10.1158/2326-6066.CIR-26-0211/3849116/cir-26-0211.pdf by guest on 22 November 2026

Significance

Th1/Th2 immune polarization regulates cancer stem cell properties and therapeutic resistance. While robust IFNγ signaling suppresses cancer cell stemness and enhances treatment sensitivity, low-intensity IFNγ signaling or IL-4 promote stem-like, drug-resistant phenotypes.

Downloaded from aacrjournals.org/cancerimmunolres/article-pdf/doi/10.1158/2326-6066.CIR-26-0211/3849116/cir-26-0211.pdf by guest on 22 November 2026

INTRODUCTION

The role of innate and adaptive immune responses has been widely studied in the context of tumor development, indicating the necessity of a pre-existing antitumor immune contexture for the efficacy of clinical responses. A general consensus indicates that in most cancers the prevalence of cytotoxic T cells and Th1 cells is associated with a better prognosis [1,2], while a high density of M2-skewed myeloid suppressor cells, including tumor-associated macrophages (TAMs) and myeloid-derived suppressor cells (MDSCs), correlates with a poor prognosis [2–4].

In the interplay between the opposing roles of lymphoid and myeloid activation states, the accumulation of immunosuppressive myeloid populations appears to dominate the final outcome, interfering with the antitumor functions of T cells through several mechanisms, including secretion of IL-10, TGFβ, prostaglandins and indoleamine 2,3- dioxygenase (IDO), expansion of both regulatory T (Treg) cells and immature and tolerogenic dendritic cells, as well as high expression of immune-checkpoint molecules (PDL1, PDL2, B7- H4) causing T cell exhaustion [5]. In agreement, several lines of evidence indicate that antitumor reprogramming of TAMs results in restoration of specific antitumor immunity [5–8].

Of relevance, the myeloid/lymphoid balance also crucially controls the biology of cancer cells [4,9], further underlining its relevance to the aggressive nature of tumors [10]. In this regard, cancer stem cells (CSC), which represent a minor fraction of tumors, provide a major obstacle to antitumor therapy [11,12], limiting clinical responses and increasing the frequency of disease recurrence [13].

Building on this background, available evidence indicates that CSC biology is of crucial interest for possible clinical developments [14], due to their ability to orchestrate tumor immune evasion, tumor vascularization and metastasis formation through the pathways and mechanisms of the "epithelial-mesenchymal transition" (EMT) process [15,16].

Of note, in addition to orchestrating the tumor microenvironment [17,18], TAMs play a crucial role in the formation of a protective niche for cancer stem cells (CSC) [19,20], producing specific biological mediators that promote developmental pathways towards cancer cell stemness [21–23]. Further, these pro-stem properties of macrophages are enhanced by the M2-like polarization state [24,25], generally associated with Th2 skewing and poor prognosis [2].

Since the specific contribution of different immune subsets to CSC plasticity is not yet fully defined and antitumor reprogramming of TAMs has been associated with the reactivation of specific antitumor Th1 immunity [6–8,26], we investigated the influence of myeloid and lymphoid activation status on the protumorigenic properties of CSC and resistance to therapy.

MATERIAL AND METHODS

Cell lines. The following mycoplasma-free cell lines were used: 3-MCA-derived sarcoma cell line MN/MCA-1, melanoma cells B16/F10 (RRID: CVCL_0159, catalog n° CRL-6475) and YUMM1.7 (RRID:CVCL_JK16, catalog n° CRL-3362). The 3-MCA-derived sarcoma cell line MN/MCA-1 was derived from stock periodically renewed through primary cells isolated from tumors implanted in WT mice, as previously described; B16/F10 and YUMM1.7 cells were purchased from ATCC (RRID:SCR_001672) in 2020. Upon receipt, cells were expanded and cryopreserved to establish working stocks. Cells were used at low passage and were not maintained in culture for more than approximately 15 passages before use. B16/F10 and YUMM1.7 cells were obtained from a commercial supplier that performs cell line characterization; reauthentication was not performed. Mycoplasma contamination was routinely monitored by PCR and the cell lines used in this study were confirmed to be Mycoplasma-free. No additional genetic manipulation, including GFP

Downloaded from aacrjournals.org/cancerimmunolres/article-pdf/doi/10.1158/2326-6066.CIR-26-0211/3849116/cir-26-0211.pdf by guest on 22 November 2026

expression, overexpression, gene deletion or knockdown, was performed on the cell lines used in this study. 3-MN/MCA-1 were *in vitro* cultured in RPMI-1640 medium (Euroclone, catalog n° ECB9006L) supplemented with 10% fetal bovine serum (FBS, Euroclone, catalog n° ECS0816L), 100U/ml Penicillin/Streptomycin (Euroclone, catalog n° ECB3001D) and 2mmol/L glutamine (Euroclone, catalog n° ECB3004D). B16/F10 cells were cultured in DMEM high glucose medium (Sigma-Aldrich, catalog n° D5671) supplemented with 10% fetal bovine serum (FBS, Euroclone, catalog n° ECS0816L), 100 U/ml penicillin/streptomycin (Euroclone, catalog n° ECB3001D) and 2mmol/L glutamine (Euroclone, catalog n° ECB3004D). YUMM1.7 cells were cultured in DMEM/F12 medium (Euroclone, catalog n° ECM0090L), supplemented with 10% fetal bovine serum (FBS, Euroclone, catalog n° ECS0816L), 100 U/mL Penicillin/Streptomycin (Euroclone, catalog n° ECB3001D), MEM non-essential amino acids (Euroclone, catalog n° ECB3054D), 2mmol/L glutamine (Euroclone, catalog n° ECB3004D), 25mM Hepes (Sigma-Aldrich, catalog n° H0887). Cells were cultured at 37 °C, 5% CO_2 and harvested at confluence using trypsin-EDTA (Euroclone, catalog n° ECM0920D).

Spheroid-forming cell culture. Cells were plated in poly-2-hydroxyethyl methacrylate (pHEMA, Sigma-Aldrich, catalog n° P3932)-coated tissue culture treated plates (Corning, New York, NY, USA) in serum-free DMEM/F12 medium (Euroclone, catalog n° ECM0090L), supplemented with 100 U/mL Penicillin/Streptomycin (Euroclone, catalog n° ECB3001D), 2mmol/L glutamine (Euroclone, catalog n° ECB3004D), bovine serum albumin (BSA, 4 mg/mL; Sigma-Aldrich, catalog n° A7030), human bFGF (20 ng/mL, Gibco, catalog n° PHG0369V), human EGF (20 ng/mL, STEMCELL, catalog n° 78006.2), insulin (5 µg/mL, SigmaAldrich, catalog n° I2643), heparin (0.625 U.I/mL, PharmaTex, Milan, Italy, catalog n° 034692018), and B27 (GIBCO, catalog n° 17504-044) at a density of 5×10^4 cells/well. Medium was replaced every 7 days.

According to the experimental design, MN/MCA-1, B16/F10 (RRID: CVCL_0159) and YUMM1.7 (RRID:CVCL_JK16) cells were cultured in spheroid-forming conditions in the presence of IFNγ

Downloaded from aacrjournals.org/cancerimmunolres/article-pdf/doi/10.1158/2326-6066.CIR-26-0211/3849116/cir-26-0211.pdf by guest on 22 November 2026

(Peprotech, 20ng/ml or 0,2 ng/ml, catalog n° 315-05-100UG) or IL-4 (20ng/ml, Peprotech, catalog n° 214-14-100UG) or left untreated for one week and then subjected to subsequent analysis. After one week, where indicated, spheroids were treated with doxorubicin (1 μM, Sigma-Aldrich, catalog n° D1515) or PLX4032 (10 μM, MedChemExpress, catalog n° HY-12057). Where indicated, cells were pretreated with the indicated inhibitors, including PF04691502 (1 μM, MedChemExpress, catalog n° HY-15177) and Ruxolitinib (1 μM, MedChemExpress, catalog n° HY-50856), for 1 hour before IFNγ treatment; treatments were repeated on days 3 and 5, for a total of 6 days.

Extreme limiting dilution assay (ELDA). To determine the frequency of spheroid-forming cells, cells were plated at different concentrations in 96-well flat-bottom ultra-low attachment pHEMA-coated plates in a total volume of 0.1 ml of serum-free DMEM/F12 medium supplemented as for spheroid cultures. Fifteen replicate wells were set up for each cell concentration. After a week, the wells were scored for spheroid formation; the frequency of spheroid-forming precursors in each population was calculated by ELDA web tool (http://bioinf.wehi.edu.au/software/elda). Data were expressed as the number of spheroid-forming cells/10^3 cells.

Tumor supernatant preparation. Tumors were disaggregated and reduced to single cell suspension, (as described in detail in murine sample processing section) and then were plated in a Petri dish in 10ml of RPMI-1640 complete medium, at a concentration of 40×10^6 cells. After 24h, the medium was collected and centrifuged at 3000rpm 15min RT to eliminate cells from the suspension. The resulting tumor supernatant was then collected at -20°C and used at 1:1 ratio with complete or spheroid-forming medium (according to the experimental design).

ELISA. Murine IL6 (catalog no. DY406, RRID:AB_3068344) and TNFα (catalog no. DY410, RRID:AB_3752046) were quantified using R&D DuoSet ELISA Development Systems. Murine IFNγ was quantified using Invitrogen kit (catalog no. BMS609).

Downloaded from aacrjournals.org/cancerimmunolres/article-pdf/doi/10.1158/2326-6066.CIR-26-0211/3849116/cir-26-0211.pdf by guest on 22 November 2026

The following human cytokines were measured in serum of cancer patients and healthy donors: IL-2, IFNγ, IL-10, IL-12p70, IL-6, TNFα. Serum was initially diluted 1:2. We used the Ella 600-100 (R&D Systems) automated enzyme-linked immunosorbent (ELISA) platform. This performs a sandwich ELISA using a microfluidics Simple Plex cartridge. This immunoassay works by routing the sample through a microfluidic channel that binds the protein of interest. The unbound analyte is removed by washing, before a detection antibody is added. Because each channel has three glass nano reactors coated with a capture antibody, a triplicate set of results are produced for each sample. Results were then generated using the manufacturer-calibrated standard curve.

Scratch assay. MN/MCA-1 cells were plated in untreated six-well plates. When at confluence, cells were scratched with a p200 pipet tip. Wells were washed to remove detached cells, and medium was replaced with completed RPMI-1640 medium alone or with tumor supernatant (TSN, ratio 1:1) from the tumors grown in the different mouse models. At time 0 and after 24 and 48h, pictures of the wounded area were taken with Leica DM IL LED microscope (Wetzlar, Germany). The distance between scratch edges was quantified using ImageJ software (RRID: SCR_003070).

Transwell migration assay. Tumor cells were pretreated for 48h with tumor supernatants (TSN) collected from $p50^{fl/fl}$ or $p50^{fl/fl}$*Tie2-Cre* tumors. Following pretreatment, 5*10^5 cells were harvested and seeded into the upper chamber of 8-µm pore-size Transwell inserts (Corning, catalog n°3422) in serum-free medium. The lower chamber contained complete medium supplemented with TSN from $p50^{fl/fl}$ mice. After 24 h of incubation at 37°C in a humidified 5% CO_2 atmosphere, non-migrated cells were removed from the upper surface of the membrane using a cotton swab. Cells that had migrated to the lower surface were fixed and stained with crystal violet. The dye retained by migrated cells was subsequently solubilized, and cell migration was quantified by measuring the absorbance at 570 nm using a microplate reader.

Downloaded from aacrjournals.org/cancerimmunolres/article-pdf/doi/10.1158/2326-6066.CIR-26-0211/3849116/cir-26-0211.pdf by guest on 22 November 2026

Animals. All mice used in this study were 8–12 weeks of age, and both males and females were used. Individual experiments were age and sex matched. Wild-type C57BL6/J mice were obtained from Charles River Laboratories (RRID: MGI:3028467). NF-κB1/p50-deficient mice were available in-house [6]. NFKB1flox/flox ($p50^{fl/fl}$) mice were generated in our laboratory [7]. $p50^{fl/fl}$ mice were crossed with B6.Cg-Tg(Tek-Cre)1Ywa (Jackson Laboratories, RRID:IMSR_JAX:008863) to generate $p50^{fl/fl}$*Tie2-Cre* mice. All colonies were housed and bred in the specific-pathogen-free animal facility at the Humanitas Clinical and Research Center (Rozzano, Milan, Italy) in individually ventilated cages. Mice were housed under a 12/12-h light/ dark cycle at an ambient temperature of 22 ± 1 °C with humidity 52–55%. Mice were randomized based on sex, age and weight. In most in vivo experiments, the investigators were unaware of the genotype of the experimental groups. Sample sizes were defined on the basis of our many years of experience with the experimental models used in our study, in order to detect differences of 20% or greater between the groups (10% significance level and 80% power). All procedures involving handling and care of mice were conducted in accordance with applicable national and international regulations and institutionals guidelines; in particualr, the animal experiments were reviewed and approved by the Humanitas Clinical and Research Center and in accordance with national (Legislative Decree no. 116, G.U., Supplementary 40, 02-18-1992 and no. 26, G.U., 03-04-2014) and international law and policies (EEC, Council Directive nos. 2010/63/EU, OJ L276/33 and 09-22-2010; National Institutes of Health Guide for the Care and Use of Laboratory Animals, US National Research Council, 2011). The study was approved by the Italian Ministry of Health (nos. 97/2014-PR, 25/2018-PR, n° 339/2024-PR). All efforts were made to minimize the number of animals used and their suffering.

Cancer models. Mice were injected intramuscularly into their left hindlimb with 3-MCA-derived, mycoplasma-free sarcoma cell line MN/MCA-1 (10^5 cells per mouse in 100 µl of PBS). From day 14 after tumor cell injection, primary tumor growth was monitored three times per week with a caliper. For melanoma models, mice were subcutaneously injected with 100 µl of PBS containing

Downloaded from aacrjournals.org/cancerimmunolres/article-pdf/doi/10.1158/2326-6066.CIR-26-0211/3849116/cir-26-0211.pdf by guest on 22 November 2026

5×10^5 murine melanoma B16/F10 cells. Ten days after tumor cell injection, tumor growth was monitored three times per week with a caliper. To study tumorigenic potential of CSC, ckit$^+$ and ckit$^-$ cells were FACS sorted from MN/MCA-1 spheroids and injected subcutaneously into mice at different numbers (according to the experimental design).

***In vivo* treatments.** When specified, starting from the day before tumor injection, mice received an intraperitoneal injection of 0.3 mg of anti-mouse CD4 (Rat Anti-Mouse CD4 Monoclonal Antibody, Unconjugated, Clone GK1.5, BioXcell, catalog n° BE0003-1, RRID:AB_1107636) once per week for the duration of the experiment. FACS analysis of peripheral blood samples confirmed depletion of CD4$^+$ cells over 7 days. Starting from day 7 after tumor cell injection, MN/MCA-1-bearing mice received intraperitoneal treatment with the following reagents: anti-IFNγ monoclonal antibody (BioXcell, Clone XMG1.2, catalog n° BE0055, RRID:AB_1107694) at a dose of 200 μg/mouse twice a week; anti-PD-1 monoclonal antibody (BioXcell, Clone RPM1-14, catalog n° BE0146, RRID:AB_10949053) at a dose of 100 μg/mouse, twice a week; anti-IL-4 monoclonal antibody (BioXcell, Clone, 11B11, catalog n° BE0045, RRID:AB_1107707) at a dose of 200 μg/mouse twice a week. When specified, from day 7 after tumor cells injection, MN/MCA1-bearing mice were intratumorally injected with 1 μg/mouse of recombinant IFNγ cytokine (Peprotech, catalog n° 315-05-100UG), three times a week for the duration of the experiment. When specified, starting from 10 days after cell injection, MN/MCA-1-bearing mice were intravenously injected with doxorubicin (Sigma-Aldrich, catalog n° D1515) at a dose of 1 mg/Kg twice a week.

Lung histology. Lungs were collected following intracardiac perfusion with cold PBS and were formalin fixed for 24 h, dehydrated and paraffin embedded for histologic analysis. Histology was performed on longitudinal serial sections (100 μm apart, width 8 μm) from each lung, stained with hematoxylin and eosin (H&E) and scanned using a VS120 Dot-Slide BX61 virtual slide microscope (Olympus Optical, RRID: SCR_018411). The area of lung lesions was obtained by manual tracing

Downloaded from aacrjournals.org/cancerimmunolres/article-pdf/doi/10.1158/2326-6066.CIR-26-0211/3849116/cir-26-0211.pdf by guest on 22 November 2026

of the perimeter of lesions using Image Pro-Premiere software 9.2 (Media Cybernetics, RRID: SCR_016497).

Murine sample processing. According to the experimental design, at the sacrifice of the animals, tumors, spleens and whole blood were collected. Primary tumors were cut into small pieces, disaggregated with 0.5 mg/ml COL IV (Sigma-Aldrich, catalog n° C5138) and 150 U/ml DNase I (Roche, catalog n° 70271500) in RPMI 1640 for 30 min at 37 °C and filtered through strainers. Macroscopic lung metastatic lesions were removed with tweezers. Pulmonary nodules isolated were finely minced, disaggregated with 0.5 mg/ml COL IV and 150 U/ml DNase I in RPMI 1640 for 30 min at 37 °C and filtered through Falcon strainers (70 μm). Splenocytes were collected from spleens after disaggregation and filtration through Falcon strainers (70 μm). Whole blood samples were collected from the facial vein or heart in EDTA-coated collection tubes and directly processed using a standardized red blood cell lysis protocol. Once obtained a single cell suspension, cells were resuspended in Hank's balanced salt solution (Euroclone, catalog n° ECM0507L) supplemented with 0.5% bovine serum albumin (BSA, Sigma-Aldrich, catalog n° A7030).

Flow Cytometry (FACS) analysis. Cells were resuspended in Hank's balanced salt solution ((Euroclone, catalog n° ECM0507L) supplemented with 0.5% bovine serum albumin (BSA, Sigma-Aldrich, catalog n° A7030) and 2mM EDTA (Sigma-Aldrich, catalog n° E0270). Staining was performed at 4 °C for 20 min with the following mouse antibodies: CD45-PerCP (30-F11) (1/200, Biolegend catalog no. 103130, RRID:AB_893339); CD45-BUV563 (30-F11) (1/400, BD Horizon catalog no. 565710, RRID:AB_2722550); CD11b-BV711 (M1/70) (1/600, Biolegend catalog no. 101242, RRID:AB_2563310); F4/80-PE-Cy7 (BM8) (1/200, Biolegend catalog no. 123114, RRID:AB_893478); Ly6G-BV570 (1A8) (1/100, Biolegend catalog no. 127629, RRID:AB_10899738); Ly6C- APC-Cy7 (HK1.4) (1/600, eBioscence catalog no. 47-5932-82, RRID:AB_2573992); MHCII-PE (M5/114.15.2) (1/400, Biolegend catalog no. 107607,

Downloaded from aacrjournals.org/cancerimmunolres/article-pdf/doi/10.1158/2326-6066.CIR-26-0211/3849116/cir-26-0211.pdf by guest on 22 November 2026

RRID:AB_313322); CD20-PE-Cy7 (1/400, Biolegend catalog n° 150420. RRID:AB_2721674); MHCII-BV480 (M5/114.15.2) (1/600, BD Horizon catalog no. 566088, RRID:AB_2869739); CD11c-APC (N418) (1/100, Biolegend catalog no. 117310, RRID:AB_313779); CD11c-BV605 (N418) (1/200, eBioscence catalog no. 63-0114-82, RRID:AB_2722930); CD8-BUV805 (53-6.7) (1/200, BD Horizon catalog no. 564920, RRID:AB_2716856); CD4-PE (GK1.5) (1/200, Biolegend catalog no. 100408, RRID:AB_312693); CD4-BUV496 (GK1.5) (1/100, BD Horizon catalog no. 564667, RRID:AB_2722549); CD3-BV650 (145-2C11) (1/100, Biolegend catalog no. 100229, RRID:AB_11204249); CD31-PE (MEC 13.3) (1/100, BD Pharmingen catalog no. 553373, RRID:AB_394819); SiglecF-FITC (S17007L) (1/100, Biolegend catalog no. 155504, RRID:AB_2750233); E-Cadherin-BV421 (DECMA-1) (1/100, Biolegend catalog no. 147319, RRID:AB_2750483); IFNγ-FITC (XMG1.2) (1/100, Biolegend catalog no. 505806, RRID:AB_315400); TNFα-Alexa Fluor 647 (MP6-XT22) (1/100, BD Pharmingen catalog no. 557730, RRID:AB_396838); CD19-PE-Cy7 (6D5) (1/200, Biolegend catalog no. 115519, RRID: AB_313654), NK1.1-APC (PK136) (1/100, Biolegend catalog no. 108710, RRID: AB_313397), CD117 (c-kit)-PE-Cy7 (2B8) (1/200, Biolegend catalog no. 105814, RRID:AB_313223); T-bet-BV421 (4B10) (1/100, Biolegend catalog no. 644832, RRID:AB_2686976); GATA-3-PE (16E10A23) (1/200, Biolegend catalog no. 653803, RRID:AB_2562722); EpCAM-PE-Cy7 (G8.8) (1/200, Biolegend catalog no. 118215, RRID:AB_1236477); iNOS-FITC (CXNFT) (1/100, eBioscence catalog no. 53-5920-82, RRID:AB_2574423); MHCII-BV711 (M5/114.15.2) (1/200, Biolegend catalog no.107643, RRID:AB_2565976); IL-12 PE-Cy7 (C15.6) (1/200, Biolegend catalog no. 505210, RRID:AB_ 2565645); IL-4-PE-Dazzle594 (1/200, Biolegend catalog no. 504132, RRID:AB_ 2564559); CD163-BV711 (TNKUPJ) (1/200, Invitrogen catalog no. 67-1631-82, RRID:AB_2784887); CD206-APC (C086C2) (1/100, Biolegend catalog no.141708, RRID:AB_10900231); HO-1-PE (HO1-2) (1/200, EnzoLifeSciences catalog no. ADI-OSA-111PE-F, RRID:AB_ 10616512). We also used unconjugated Vimentin rabbit monoclonal antibody (SP20) (1/100, ThermoFisher catalog no. MA5-14564, RRID: AB_2537928); N-Cadherin rabbit

Downloaded from aacrjournals.org/cancerimmunolres/article-pdf/doi/10.1158/2326-6066.CIR-26-0211/3849116/cir-26-0211.pdf by guest on 22 November 2026

monoclonal antibody (3B9) (1/100, ThermoFisher catalog no. 33-3990, RRID: AB_2313779) followed by incubation with secondary goat anti-rabbit Alexa Fluor 488-conjugated antibodies (1/500, ThermoFisher catalog no. A-11008, RRID: AB_143165) and goat anti-rabbit Alexa Fluor 647-conjugated antibodies (1/500, ThermoFisher catalog no. A27040, RRID: AB_2536101).

Cell viability was determined by either Aqua LIVE/Dead-405-nm staining (1/800, Biolegend catalog no. 423102) or LIVE/DEAD Fixable Violet Dead Cell Stain Kit (1/1,000, ThermoFisher catalog no. L34960); negative cells were considered viable. A Foxp3/Transcription Factor Staining Buffer Set (eBioscience, catalog n° 00-5523-00) was used for intracellular staining of TNFα, IFNγ, iNOS, c-kit, Tbet, GATA3. Expression of TNFα, IFNγ and iNOS was analyzed by flow cytometry following 4 h of treatment with brefeldin A (5 µg/ml, Sigma-Aldrich, catalog n° B7651), PMA (50 ng/ml, Sigma-Aldrich, catalog n° P8139) and ionomycin (1 µg/ml, Sigma-Aldrich, catalog n° I0634). Cells were detected using either BD LSRFortessa (RRID: SCR_018655) or BD FACSymphony A5 (RRID: SCR_022538) and analyzed with FlowJo software (v9.9.6 and v10.9.0) (RRID: SCR_ 008520) software. Results are reported as MFI normalized on isotype control or fluorescence minus one. For t-distributed stochastic neighbor embedding (tSNE) analysis, a unique computational barcode was assigned to single samples. Events gated on live $CD45^+$ cells were subsequently concatenated and visualized with tSNE visualization (Barnes-Hut implementation; iterations, 1000; perplexity, 20; initialization, deterministic; theta, 0.5; eta: 200).

Annexin V/Propidium Iodide (PI) assay. Cell death was quantified by dual Annexin V/propidium iodide (PI) staining followed by multiparametric flow cytometric analysis. Where indicated, after treatment, cells were harvested, washed twice with ice-cold phosphate-buffered saline (PBS, pH 7.4, Microgem, catalog n° PBSAVHMY-500ML) and resuspended in 1× Annexin V binding buffer (Immunostep, catalog n° ANXVKF-100T) at a final concentration of 10^6 cells/mL. Annexin V–FITC (Immunostep, catalog n° ANXVKF-100T) and PI (Immunostep, catalog n° ANXVKF-100T) were added according to the manufacturer's instructions and samples were incubated for 15 min at

Downloaded from aacrjournals.org/cancerimmunolres/article-pdf/doi/10.1158/2326-6066.CIR-26-0211/3849116/cir-26-0211.pdf by guest on 22 November 2026

room temperature in the dark. Following incubation, samples were immediately analyzed using a BD LSRFortessa flow cytometer (BD Biosciences) equipped with FACSDiva software (RRID:SCR_001456). Data were processed using FlowJo software (v10.9.0, RRID:SCR_008520). Based on Annexin V and PI fluorescence, four distinct cell populations were identified: viable cells (Annexin V^-/PI^-), early apoptotic cells (Annexin V^+/PI^-), late apoptotic cells (Annexin V^+/PI^+), and necrotic cells (Annexin V^-/PI^+).

In vitro **Induction of Th1 and Th2 Cell Polarization.** To obtain high-purity naïve $CD4^+$ cells ($CD44^-CD62L^+$), single cell suspension obtained from the spleens harvested from naïve mice (as described in detail in murine sample processing section) were further stained with LIVE/DEAD Fixable Violet Dead Cell Stain Kit (1/1,000, ThermoFisher catalog no. L34960), CD45-PerCP (30-F11) (1/200, BioLegend, catalog no. 103130, RRID:AB_893339), CD3-BV711 (145-2C11) (1/400, BioLegend, catalog no. 100349, RRID: AB_2565841), CD4-PE-Cy7 (GK1.5) (1/200, BioLegend, catalog no. 100422, RRID: AB_11149488), CD8-APC (53-6.7) (1/100, BioLegend, catalog no. 100712, RRID: AB_312751), CD44-FITC (IM7) (1/100, BioLegend, catalog no.103006, RRID: AB_312957), CD62L-BV570 (Mel-14) (1/100, BioLegend, catalog no. 104433, RRID: AB_10900262) and sorted using a FACSAria cell sorter (BD Bioscience). The purity of each population was ≥90%. To induce Th cell polarization, naïve $CD4^+$ T cells were cultured in 6-wells precoated with anti-CD3ε (10 μg/mL; clone 145-2C11, Biolegend, catalog n° 100340) in the presence of IL-2 IS (10 ng/mL; 50 U/ml, Miltenyi, catalog n° 130-120-331) and anti-CD28 in soluble form (1 μg/mL; clone 37.51, BD Pharmingen, catalog n° 553294, RRID:AB_394764). In Th1-polarizing cultures, IL-12 (10 ng/mL; 60 U/ml, Miltenyi, catalog n° 130-096-707) and IL-4-blocking antibody (10 μg/mL; Miltenyi, catalog n° 130-095-709) were also added. In Th2-polarizing cultures, IL-4 (10 ng/mL; 200 U/ml, Miltenyi, catalog n° 130-097-761) and IFNγ-blocking antibody (10 μg/mL Miltenyi, catalog n° 130-095-729) were added. Cells were incubated at 37 °C and 5–10% CO_2 for up to 6 days. and subsequently used for in vitro spheroid-forming

Downloaded from aacrjournals.org/cancerimmunolres/article-pdf/doi/10.1158/2326-6066.CIR-26-0211/3849116/cir-26-0211.pdf by guest on 22 November 2026

assays. At day 3, half of the medium was replaced with fresh medium containing the differentiation cocktails.

Co-culture assays. $CD4^+$ cells were isolated from the single cell suspension obtained from the spleens and the tumors harvested from tumor-bearing mice (as described in detail in murine sample processing section). The cell suspension was enriched in $CD4^+$ cells through positive selection using CD4 microbeads (MACS, Miltenyi Biotec, catalog n° 130-117-043), according to the magnetic separation protocol. The purity of $CD4^+$ cells was ~90% as determined by FACS. The resulting cells were used for co-culture assays. In detail, splenic and tumor $CD4^+$ cells were added to the culture in a ratio of 3:1 with MN/MCA-1 cells. After 24 and 48h cell viability and c-kit expression among $CD45^-$ cells was evaluated by FACS. After 48h MN/MCA-1 cells were collected and plated in spheroid-forming cell culture for 1 week.

T cell suppression assay. A total of 2× 10^5 splenocytes from naïve wt mice were labeled with 1μmol/L of CellTrace CFSE (Life technology, catalog n° C345534) for 10 min at 37 °C protected from light. Subsequently, cells were washed, resuspended in RPMI 1640 complete medium, and seeded on wells coated with anti-CD3 (3 μg/ml, 2C11, Biolegend, catalog n° 100340, RRID: AB_2800555) and anti-CD28 antibodies (2 μg/ml, 37.5, BD Pharmingen, catalog n° 553294). To isolate M-MDSC, splenocytes were collected from spleens after disaggregation and filtration through Falcon strainers (70 μm). The cell suspension was enriched in $CD11b^+$ cells through positive selection using CD11b microbeads (MACS, Miltenyi Biotec, catalog n° 130-097-142). The purity of $CD11b^+$ cells was ~90% as determined by FACS. To obtain high-purity M-MDSC populations, $CD11b^+$ cells were further stained with LIVE/DEAD Fixable Violet Dead Cell Stain Kit (1/1,000, ThermoFisher catalog no. L34960), CD45-PerCP (30-F11) (1/200, BioLegend, catalog no. 103130, RRID:AB_ 893339), CD11b-BV711 (M1/70) (1/600, BioLegend, catalog no. 101242, RRID:AB_2563310), Ly6C-APC-Cy7 (HK1.4) (1/600, eBioscience/Thermo Fisher

Downloaded from aacrjournals.org/cancerimmunolres/article-pdf/doi/10.1158/2326-6066.CIR-26-0211/3849116/cir-26-0211.pdf by guest on 22 November 2026

Scientific, catalog no. 47-5932-82, RRID:AB_2573992), Ly6G-PE (1A8) (1/100, BioLegend, catalog no. 127607, RRID:AB_1186104) and sorted using a FACSAria cell sorter (BD Bioscience). The purity of each population was ≥90%. The resulting FACS-sorted M-MDSC were co-cultured with CFSE-labeled splenocytes at different ratios of myeloid cells:splenocytes (25% and 50%). After 72 h of co-culture, cells were collected, stained with anti-CD4 APC (Biolegend, catalog n° 100412, RRID: AB_312697) and anti-CD8 PE-Cy7 (Biolegend, catalog n° 100721, RRID:AB_312760), and analyzed by flow cytometry. CellTrace signal from anti-CD3/CD28-activated lymphocytes, which were not co-cultured with myeloid cells, was used to evaluate cell proliferation.

Quantitative RT-PCR analysis. Total RNA was extracted from the experimental cell populations indicated in the corresponding figure legends using TRIzol reagent (Invitrogen, catalog n° 15596018) following the manufacturer's instructions. RNA quality was assessed by measuring the 260/280 and 260/230 absorbance ratios. For each sample, 1 μg of total RNA was reverse transcribed using a High Capacity cDNA Archive Kit (Applied Biosystems, catalog n° 4368813); for quantitative real-time PCR, 16 ng of cDNA was used as template for each reaction. qRT-PCR was performed using SybrGreen PCR Master Mix (Applied Biosystems, catalog n° 1725274, RRID: SCR_023358) in a 7900HT Fast Real-Time System (Applied Biosystems) and ViiA-7 Fast Real-Time System (Applied Biosystems). All samples were analyzed in technical duplicates. Data were processed using SDS v.2.2.2 or ViiA™ 7 Software (Applied Biosystems, RRID: SCR_023358) and analyzed with the $2^{(-\Delta CT)}$ method. Data were normalized to 18S rRNA expression and represented as fold change relative to the control group. The genes analyzed included stemness-associated genes (*Nanog, Sox2, Oct4, c-kit, ALDH*), EMT-associated genes (*Cdh1, Cdh2, Vimentin, Snail, ZEB1*), and immune polarization-associated genes (*Fasl, Gzmb, Il12A, IFNγ, Stat1, Tbx21, TNFα, Prf1, Il21, Ccl5, TGFβ, IL-12p40*), as indicated in the corresponding figures. The sequences of gene-specific primers were obtained from previous published papers [8, 30, 31] or were designed

Downloaded from aacrjournals.org/cancerimmunolres/article-pdf/doi/10.1158/2326-6066.CIR-26-0211/3849116/cir-26-0211.pdf by guest on 22 November 2026

by using NCBI Primer-BLAST. Gene-specific primers were synthesized by Sigma-Aldrich. Primer sequences, including the forward and reverse sequences for each gene, are provided in Supplementary Table S1.

Patients. To measure circulating cytokines, human peripheral sera were isolated from healthy donors (n=20), sarcoma patients (n=44) and melanoma patients (n=19) at the Humanitas Research Hospital between 2020 and 2025. Serum samples were collected before surgical removal of the primary tumor and stored at -80°C until analysis. In detail, the following sarcoma histotypes were recruited: dedifferentiated liposarcoma (n=19), leiomyosarcoma (n=12), undifferentiated pleomorphic sarcoma (n=4), gastrointestinal stromal tumors (n=5), rhabdomyosarcoma (n=1), sarcoma epithelioid (n=2), chondrosarcoma (n=1). Samples from the sarcoma cohorts described in this study were obtained before surgically removal of primary tumor with written informed consent from the patients. The study was conducted according to the Declaration of Helsinki Principles and following approval by the Ethics Committee of Humanitas Research Hospital, Milan, Italy. According to favorable or poor prognosis after surgery, patients were then stratified in two groups: no evidence of disease (NED) and dead or alive with disease (AWD).

External datasets. Statistical analyses on external sarcoma and melanoma datasets were performed using R statistical software (version 4.5.2).

Raw gene expression data for the sarcoma dataset (TCGA-SARC) were downloaded from TCGA and normalized using Deseq2 package (RRID:SCR_015687), whereas TPM-normalized values for the melanoma dataset Metastatic Melanoma, DFCI, Nature Medicine 2019; cBioPortal study ID: mel_dfci_2019) were downloaded directly from cBioportal; in both cases, data were log2-transformed.

Univariable and multivariable Cox proportional hazards regression analyses were performed using the survival package to assess the prognostic value of individual TH1 genes and gene combinations. For each multivariable model, a risk score was calculated as the sum of each gene's expression

Downloaded from aacrjournals.org/cancerimmunolres/article-pdf/doi/10.1158/2326-6066.CIR-26-0211/3849116/cir-26-0211.pdf by guest on 22 November 2026

level multiplied by its corresponding regression coefficient. Kaplan–Meier survival curves were generated, and differences between groups were assessed using the log-rank test. Survival plots, including number-at-risk tables, were generated using the survminer package. Patients were stratified according either to the median expression of single Th1 genes or to the median of the risk score given by the Cox regression models.

Boxplots were generated to compare the distribution of selected gene expression levels (e.g., SOX2, ZEB1, NANOG) between IFNγ-high and IFNγ-low patient groups. Plots were created using ggplot2 package (RRID:SCR_014601) and statistical significance was evaluated using a two-sided Wilcoxon rank-sum test. Correlations analysis to investigate the relationships between the expression levels of Th1 genes and ZEB1 were performed using Spearman's rank correlation coefficient. Correlation matrices and hierarchical clustering results were visualized as heatmaps using the pheatmap package (RRID:SCR_016418) and the ggcorrplot package. The associations between Th1 signature and ZEB1 expression were further illustrated with scatterplot including fitted linear regression line; Spearman's rank correlation coefficient and the corresponding p-value were indicated. Scatterplots were generated using the ggpubr package.

Statistical information. Statistical analysis was performed using GraphPad Prism v.8.2.1 software (RRID: SCR_002798). P-values below 0.05 were considered statistically significant. The results are represented as mean ± SEM, unless otherwise stated. Statistical significance is indicated in each graph. For the experiments comparing two independent grouping variables, two-way analysis of variance (ANOVA) was applied, and Šidák's or Tukey's multiple-comparisons tests were performed based on the nature of the comparison. Data with more than two independent groups were analyzed using one-way ANOVA or Kruskal-Wallis, depending on the specific experimental design. When comparing only two groups, an unpaired t-test or Mann-Whitney test was applied, depending on the nature of data distribution. No data were excluded from the analysis. The number of biological replicates and the statistical methods used are specified in all figure legends.

Downloaded from aacrjournals.org/cancerimmunolres/article-pdf/doi/10.1158/2326-6066.CIR-26-0211/3849116/cir-26-0211.pdf by guest on 22 November 2026

Data availability. The data generated in this study, including raw flow cytometry data, quantitative RT-PCR data and all other primary experimental data supporting the findings of this study, are available from the corresponding author upon reasonable request. The publicly available transcriptomic datasets analyzed in this study were obtained from The Cancer Genome Atlas (TCGA-SARC; 259 patients) at: https://portal.gdc.cancer.gov/ and from cBioPortal (Metastatic Melanoma, DFCI, Nature Medicine 2019, study ID: mel_dfci_2019; 121 patients) at https://www.cbioportal.org/study/summary?id=mel_dfci_2019, as described in the External datasets section of the Materials and Methods.

Code availability. The data and code used for statistical analyses and figure generation, based on publicly available sarcoma and melanoma transcriptomic datasets, are available in a Code Ocean Compute Capsule https://codeocean.com/capsule/4954248/.

RESULTS

c-kit expression identifies murine fibrosarcoma CSC.

By preliminary screening, we identified the proto-oncogene receptor tyrosine kinase c-kit [27] as a reliable marker of CSC in a preclinical model of fibrosarcoma (MN/MCA-1) [6]. Indeed, when cultured under non-adherent spheroid-forming conditions for expansion of CSC, MN/MCA-1 fibrosarcoma cells were able to form 3D spheroidal structures (Fig. 1A), enriched in the expression of c-kit (Fig. 1B left) and stemness-associated genes (i.e. Nanog, Sox2 and Oct4) [28,29] (Fig. 1B right), as compared to MN/MCA-1 cells cultured in adherent conditions. Supporting this evidence, FACS sorted c-kit$^+$ cells showed higher tumorigenic potential when injected into syngeneic mice (Fig. 1C), as well as higher expression of stemness-associated genes (Fig. 1D). Similar results were obtained in c-kit$^+$ and c-kit$^-$ cells isolated from tumors generated by intramuscular injection of MN/MCA-1 cells into syngeneic C57Bl/6 mice: c-kit$^+$ cells presented higher expression of

Downloaded from aacrjournals.org/cancerimmunolres/article-pdf/doi/10.1158/2326-6066.CIR-26-0211/3849116/cir-26-0211.pdf by guest on 22 November 2026

stemness-associated genes (Fig. 1E left) and higher spheroid-forming ability (Fig. 1E right), compared to c-kit$^-$ tumor cells.

Lack of hematopoietic p50 NF-κB compromises tumor cell stemness and metastasis formation.

To examine the impact of immune polarization on tumor cell stemness, we exploited our previous observations demonstrating that accumulation of the p50 NF-κB subunit in TAMs is a key event of their pro-tumor M2-like polarization [6,7,30] and that p50 NF-κB gene depletion reprograms their functions toward an antitumor M1 state, associated with enhanced expression of M1/Th1 cytokines/chemokines [6,31]. Based on this premise, mCherry-expressing MN/MCA-1 cells were injected into total p50-deficient mice (p50KO) and in WT mice. After 25 days, mice were sacrificed and tumors analyzed. In agreement with previous observations [6,7,31], tumor growth was slower in p50KO mice, compared to their WT counterparts (Fig. 2A). In addition, the absence of the NF-κB p50 subunit correlated with reduced CSC frequency in primary tumors, as demonstrated by a lower number of c-kit$^+$/mCherry$^+$ cells among CD45$^-$ cells (non-immune cells) (Fig. 2B, left). Ex vivo analysis of tumor cells further supported the impairment of the CSC transcriptional program, revealing significantly reduced expression of the stemness-associated genes *Nanog*, *Sox2* and *Oct4* (Fig. 2B, right). Consistent with this, MN/MCA-1 cells derived from tumors grown in p50KO mice and cultured under non-adherent conditions gave rise to a reduced number of spheroids, characterized by smaller diameters (Fig. 2C).

Since cancer cell stemness and epithelial-mesenchymal transition (EMT) are intricately linked [16], we analyzed markers of EMT [32] within c-kit$^+$ tumor cells, isolated from either WT or p50-deficient tumor-bearing mice. As a result, we observed that the lack of p50 NF-κB induced a significant increase in the expression of the epithelial marker E-cadherin (*Cdh1*), concomitantly with a reduced expression of the mesenchymal markers N-cadherin (*Cdh2*) and Vimentin (Fig. 2D).

Downloaded from aacrjournals.org/cancerimmunolres/article-pdf/doi/10.1158/2326-6066.CIR-26-0211/3849116/cir-26-0211.pdf by guest on 22 November 2026

No statistically significant difference in EMT markers was observed in non-stem tumor cells from p50KO mice (Supplementary Fig. S1A) supporting a key role for host p50 NF-kB in the EMT transition of cancer stem cells. The acquired epithelial phenotype of CSC in p50KO mice was consistent with a reduction in both lung metastases (Fig. 2E, left) and the percentage of c-kit$^+$ cells at metastatic loci, compared with WT mice (Fig. 2E, right).

To further corroborate this observation and to better investigate the role of p50 NF-κB-mediated immune response in CSC expansion, we used the B6. Cg-Tg(Tek-Cre)1Ywa deleted strain to ablate p50 in all cells of the hematopoietic lineage (p50$^{fl/fl}$*Tie2-Cre* mice) [7], while p50$^{fl/fl}$ mice were used as a control group. As shown in Fig. 2F, tumors grown in p50$^{fl/fl}$*Tie2-Cre* mice developed a predominantly M1/Th1 immune response, as evidenced by increased expression of the M1-associated cytokines IL-12p40, TNFα, and IL-1β, accompanied by a concomitant reduction in the M2-associated cytokine TGF-β in TAMs (left). This was paralleled by increased expression of the Th1-promoting transcription factor T-bet and reduced Th2-promoting transcription factor Gata3 (right) in CD4$^+$ T cells. This M1/Th1-skewed immune milieu was consistently associated with a pronounced decline in the proportion of c-kit$^+$ tumor cells within CD45$^-$ populations (Fig. 2G left). Indeed, *ex vivo* analysis of stemness-associated genes confirmed a reduced expression of *Sox2*, *Oct4* and *c-kit* (Fig. 2G right), as well as a reduced spheroid-forming ability of tumor cells harvested from p50$^{fl/fl}$*Tie2-Cre* mice (Fig. 2H). No differences were observed in *Nanog* expression. Moreover, *ex vivo* analysis of EMT markers among c-kit$^+$ cells showed a higher expression of E-cadherin and lower expression of Vimentin and N-cadherin in CSC isolated from p50$^{fl/fl}$*Tie2-Cre* mice, compared to their counterparts isolated from p50$^{fl/fl}$ mice (Fig. 2I). While the M1/Th1 shift observed in p50$^{fl/fl}$*Tie2-Cre* mice was associated with a modest although statistically significant reduction in primary MN/MCA-1 tumor growth (Fig. 2J), it was significantly associated with reduced formation of lung metastases (Fig. 2K). Of note, no significant differences in the expression of EMT markers were detected in the c-kit$^-$CD45- non-stem cell tumor counterpart (Supplementary Fig. S1B).

Downloaded from aacrjournals.org/cancerimmunolres/article-pdf/doi/10.1158/2326-6066.CIR-26-0211/3849116/cir-26-0211.pdf by guest on 22 November 2026

Consistently, similar results were also obtained in the B16/F10 melanoma mouse model. Indeed, B16/F10 spheroids obtained under non-adherent conditions (Supplementary Fig. S2A) showed a clear increase in the expression of the stemness marker CD20 compared to tumor cells cultured under adherent conditions (Supplementary Fig. S2B, left), paralleled by an increased expression of stemness markers (ALDH, Nanog, Sox2, Oct4) (Supplementary Fig. S2B, right), as also confirmed in FACS-sorted $CD20^+$ tumor cells (Supplementary Fig. S2C**).** In parallel with reduced primary tumor growth (Supplementary Fig. S2D), the percentage of CSC was reduced in tumors grown into $p50^{fl/fl}$*Tie2-Cre* mice (Supplementary Fig. S2E left). Furthermore, similar to fibrosarcoma models (Fig. 2I), CSC from tumors grown in $p50^{fl/fl}$ *Tie2-Cre* mice exhibited a reduced mesenchymal phenotype compared to $p50^{fl/fl}$ mice (Supplementary Fig. S2E right).

Finally, to functionally validate that the reduction in melanoma CSC observed under Th1-polarized conditions reflected impaired tumor-initiating potential rather than changes in CSC marker expression alone, unfractioned B16/F10 cells isolated from tumors grown in WT or $p50^{-/-}$ mice were subjected to in vivo limiting dilution transplantation assays. Tumor cells isolated from $p50^{-/-}$ tumors displayed a markedly reduced tumor-initiating capacity compared with WT-derived tumor cells, particularly at limiting cell doses (Supplementary Fig. S2F). These findings provide direct functional evidence that tumors developing under Th1-polarized conditions contain a reduced frequency of tumor-initiating cells and, together with the reduced $CD20^+$ cell population and stemness-associated gene expression (Supplementary Fig. S2C), support our observation that Th1-polarized conditions compromise the melanoma CSC compartment.

The host immune profile modulates CSC plasticity.

To further demonstrate the impact of p50-dependent polarization of the immune response on cancer cell stemness, MN/MCA-1 cells were exposed *in vitro* to supernatant (TSN) obtained from tumors explanted from $p50^{fl/fl}$ or $p50^{fl/fl}$*Tie2-Cre* mice. After 48h, we observed reduced spheroid-forming capability (Fig. 3A) and reduced expression of c-kit and stemness-related genes (Fig. 3B) in cells

Downloaded from aacrjournals.org/cancerimmunolres/article-pdf/doi/10.1158/2326-6066.CIR-26-0211/3849116/cir-26-0211.pdf by guest on 22 November 2026

exposed to $p50^{fl/fl}$*Tie2-Cre*-derived TSN. ELISA analysis confirmed that TSN derived from $p50^{fl/fl}$*Tie2-Cre* tumors exhibited significantly higher levels of the Th1-associated cytokines TNFα, IFNγ and IL-6 than TSN from $p50^{fl/fl}$ tumors (Supplementary Fig. S3A). Corroborating our previous observations (Fig. 2, Supplementary Fig. 1 and Supplementary Fig. 2), exposure to $p50^{fl/fl}$*Tie2-Cre*-derived TSN also impacted the EMT phenotype of CSC, as attested by increased expression of *E-Cadherin* (*Cdh1*) and reduced expression of *N-cadherin* (*Cdh2)* and *Vimentin*, compared to exposure to $p50^{fl/fl}$-derived TSN (Fig. 3C). Consistent with the more invasive phenotype associated with EMT, $p50^{fl/fl}$*Tie2-Cre*-derived TSN significantly reduced both scratch wound recovery (Fig. 3D) and the migratory ability of MN/MCA-1 cells in transwell assays (Supplementary Fig. S3B), compared to $p50^{fl/fl}$-derived TSN.

In order to identify the p50 NF-κB-dependent immune components regulating cancer cell stemness within the TME, we performed e*x vivo* flow cytometry analysis on primary fibrosarcoma tumors growing in $p50^{fl/fl}$ and $p50^{fl/fl}$*Tie2-Cre* mice. Notably, t-distributed stochastic neighbor embedding (t-SNE) analysis of myeloid (Fig. 3E) and lymphoid (Fig. 3F) cell subsets showed significant differences between the two genetic backgrounds. In particular, in line with our previous report [7], tumors grown in $p50^{fl/fl}$*Tie2-Cre* mice showed a lower percentage of $CD11b^{+}F4/80^{hi}$ TAMs (Fig. 3G left) and prominent expansion of $CD11b^{+}Ly6C^{hi}$ monocytic cells compared to $p50^{fl/fl}$ mice (Fig. 3G, center). No differences were observed in the percentage of dendritic cells ($CD11c^{+}MHCII^{+}$) (Fig. 3G, right). As previously described [7], flow cytometry and functional analysis of $CD11b^{+}Ly6C^{hi}$ monocytic cells demonstrated lower expression of the immunosuppressive enzyme iNOS and increased expression of the pro-inflammatory cytokine TNFα in $p50^{fl/fl}$*Tie2-Cre* mice, compared to $p50^{fl/fl}$ mice (Fig. 3H left). These changes were accompanied by reduced *in vitro* suppressive activity of $CD11b^{+}Ly6C^{hi}$ cells (Fig. 3H right), supporting the notion that nuclear accumulation of p50 NF-κB in monocytic cells controls their immunosuppressive phenotype [6,7]. These findings were further corroborated by the phenotypic profiling of TAMs, which revealed increased expression of MHCII, TNFα and IL-12, together with reduced expression of M2-associated

Downloaded from aacrjournals.org/cancerimmunolres/article-pdf/doi/10.1158/2326-6066.CIR-26-0211/3849116/cir-26-0211.pdf by guest on 22 November 2026

markers CD163, HO-1 and CD206, indicating a shift toward a more pro-inflammatory M1-like TAM state (Supplementary Fig. S3C). Coherently, analysis of the lymphoid compartment revealed a higher percentage of $CD8^+$ T cells, NK and NKT cells in tumors growing in $p50^{fl/fl}$*Tie2-Cre* mice, compared to $p50^{fl/fl}$ mice (Fig. 3I). Notably, consistent with the reduced immunosuppressive phenotype of myeloid cells, $CD4^+$ and $CD8^+$ T cells from $p50^{fl/fl}$*Tie2-Cre* tumors exhibited a higher proportion of IFNγ- (Fig. 3J) and TNFα–producing cells (Supplementary Fig. S3D) than those from $p50^{fl/fl}$ tumors. In addition, $CD8^+$ T cells also displayed enhanced GrzB expression (Fig. 3J), whereas $CD4^+$ T cells showed reduced IL-4 production (Supplementary Fig. S3D), further supporting the establishment of a Th1-polarized tumor microenvironment. Accordingly, $CD4^+$ T cells isolated from the spleens of $p50^{fl/fl}$*Tie2-Cre* tumor-bearing mice expressed significantly higher levels of *Fasl, GzbB, Il12a, IFNG, Stat1, Tbx21 (T-bet)* and *TNF* than $CD4^+$ T cells from $p50^{fl/fl}$ tumor-bearing mice (Fig. 3K), whereas no significant differences were detected in the expression of *Prf1, Il21,* and *Ccl5*.

Comparable immunological changes were also observed in the B16/F10 melanoma model. Specifically, tumors grown in $p50^{fl/fl}$*Tie2-Cre* mice exhibited reduced infiltration of TAMs ($F4/80^+CD11b^+$) together with expansion of $CD11b^+Ly6C^{hi}$ monocytes (Supplementary Fig. S4A), which displayed increased TNFα production (Supplementary Fig. S4B). Likewise, the lymphoid compartment was characterized by increased frequencies of $CD4^+$ and $CD8^+$ T cells, NK and NKT cells (Supplementary Fig. S4C), together with enhanced IFNγ production and increased Granzyme B expression by $CD8^+$ T cells (Supplementary Fig. S4D). Moreover, splenic $CD4^+$ T cells from $p50^{fl/fl}$*Tie2-Cre* tumor-bearing mice displayed a trend toward increased expression of Th1/cytotoxicity-associated genes (Supplementary Fig. S4E), supporting the predominant Th1 polarization of $CD4^+$ cells in $p50^{fl/fl}$*Tie2-Cre* tumor-bearing mice, compared to $p50^{fl/fl}$ tumor-bearing mice.

Th1-polarized $CD4^+$ cells restrain cancer cell stemness and tumorigenesis.

Downloaded from aacrjournals.org/cancerimmunolres/article-pdf/doi/10.1158/2326-6066.CIR-26-0211/3849116/cir-26-0211.pdf by guest on 22 November 2026

To evaluate whether the polarization state of $CD4^+$ T lymphocytes modulates tumor cell stemness, MN/MCA-1 cells were cocultured with $CD4^+$ cells isolated from the spleens of either $p50^{fl/fl}$ or $p50^{fl/fl}$*Tie2-Cre* tumor-bearing mice. Then, c-kit expression by tumor cells and their ability to form spheroids were assessed at different time points. Notably, after 48 h, bulk tumor cells co-cultured with splenic $CD4^+$ T lymphocytes isolated from the spleen (Fig. 4A) or from the tumor (Fig. 4B) of $p50^{fl/fl}$*Tie2-Cre* mice showed a marked reduction in the frequency of c-kit^+ cells (left), concomitant with a reduced ability to form spheroids (right). Reduced spheroid diameter was also observed when MN/MCA-1 cells were cocultured with spleen-derived $CD4^+$ T lymphocytes from naïve WT mice that were polarized *in vitro* with the specific T helper cell differentiation cocktails toward the Th1 phenotype (IL-2+IL-12+αIL-4) [33], compared to either unstimulated naïve (Th0) or Th2 (IL-2+IL-4+αIFNγ) polarized $CD4^+$ T cells (Fig. 4C).

To evaluate the *in vivo* contribution of Th1-polarized $CD4^+$ T cells to CSC control, we next depleted $CD4^+$ T cells in $p50^{fl/fl}$*Tie2-Cre* MN/MCA-1-bearing mice, using a specific α-CD4 monoclonal antibody (α-CD4). Although $CD4^+$ T-cell depletion had only a limited effect on primary tumor growth in both genotypes, a trend toward increased tumor growth was observed in $p50^{fl/fl}$*Tie2-Cre* mice, suggesting that $CD4^+$ T cells contribute to the enhanced antitumor activity associated with the Th1-polarized tumor microenvironment (Fig. 4D). Importantly, αCD4 treatment significantly increased lung metastasis formation (Fig. 4E) and the percentage of c-kit^+ tumor cells (Fig. 4F), specifically in $p50^{fl/fl}$*Tie2-Cre* mice, supporting a key role for Th1-polarized $CD4^+$ T cells in limiting tumor dissemination and CSC expansion.

Consistent with the enhanced metastasis formation, α-CD4 treatment in $p50^{fl/fl}$*Tie2-Cre* mice favored the EMT of CSC, as attested by reduced expression of E-Cadherin and the increase of Vimentin, compared to isotype control-treated $p50^{fl/fl}$*Tie2-Cre* mice (Fig. 4G). Notably, none of the aforementioned differences were observed in $p50^{fl/fl}$ mice treated with α-CD4 (Fig. 4D-G).

To further support the key role of $CD4^+$ T cell polarization in CSC regulation, bulk MN/MCA-1 cells were treated *in vitro* with prototypical Th1 (e.g. IFNγ) or Th2 (e.g. IL-4) cytokines [34], at a

Downloaded from aacrjournals.org/cancerimmunolres/article-pdf/doi/10.1158/2326-6066.CIR-26-0211/3849116/cir-26-0211.pdf by guest on 22 November 2026

dose of 20ng/ml. As a result, while IFNγ treatment reduced both spheroid diameter (Fig. 4H, center) and the frequency of c-kit$^+$ CSC (Fig. 4H, right), IL-4 increased the number of spheroids (Fig. 4H, center) and the percentage of c-kit$^+$ CSC (Fig. 4H, right). In addition, IFNγ downregulated the expression of mesenchymal markers *Zeb1, N-cadherin (Cdh2)* and *Snail1*, while upregulating the epithelial marker *E-cadherin* (*Cdh1*). Conversely, IL-4 exerted the opposite effect, enhancing the expression of mesenchymal genes and reducing *Cdh1* levels. Consistently, exposure of MN/MCA-1 cells to anti-IFNγ antibody prevented the downregulation of c-kit expression induced by TSN obtained from p50$^{fl/fl}$*Tie2-Cre* tumors (Fig. 4I). The opposing effects of IFNγ and IL-4 on CSC modulation were further confirmed in B16/F10 melanoma cells (Supplementary Fig S5A, B). Indeed, IFNγ significantly reduced spheroid size, decreased the proportion of CD20$^+$ CSC and promoted a shift toward a more epithelial phenotype, as indicated by increased E-cadherin and reduced Vimentin expression. In contrast, IL-4 increased spheroid size, expanded the CD20$^+$ CSC compartment and induced a mesenchymal transition (Supplementary Fig. S5A,B).

To investigate the clinical significance of Th1 polarization of CD4$^+$ T cells in regulating CSC and EMT programs, we analyzed publicly available transcriptomic datasets with clinical information, downloaded from The Cancer Genome Atlas (TCGA) for sarcoma and from cBioPortal (Metastatic Melanoma (DFCI, Nature Medicine 2019) dataset) for melanoma patients, and performed serum cytokine profiling in independent cohorts of sarcoma (n=44) and melanoma (n=19) following primary tumor resection (Fig. 4J-O and Supplementary Fig. S4C-F). Cox proportional hazards regression analysis of external datasets revealed that a low Th1 risk score was independently associated with improved overall survival (OS) in both sarcoma (Fig. 4J) and melanoma patients (Supplementary Fig. S5C). Because all genes included in the Th1 signature had negative Cox regression coefficients, higher expression of the Th1 signature generated lower Th1 risk scores. Accordingly, patients with low Th1 risk scores exhibited higher Th1 signature expression and improved survival, whereas high Th1 risk scores reflected lower Th1 signature expression and poorer prognosis. Kaplan–Meier analysis showed that sarcoma (Fig. 4K) and melanoma

Downloaded from aacrjournals.org/cancerimmunolres/article-pdf/doi/10.1158/2326-6066.CIR-26-0211/3849116/cir-26-0211.pdf by guest on 22 November 2026

(Supplementary Fig. S5D) patients with high IFNγ expression had significantly better overall survival than those with low IFNγ expression, further supporting the favorable prognostic value of a Th1-skewed immune response.

Consistent with our bioinformatics analysis, sarcoma patients with a favorable prognosis (NED: no clinical evidence of disease after surgical removal of the primary tumor) exhibited significantly higher levels of circulating Th1-polarizing cytokines IL-2, IL12p70 and TNFα, compared to patients with poor prognosis (AWD: dead or alive with disease after surgical removal of the primary tumor) (Fig. 4L). Serum IFNγ levels also showed a trend toward higher values in NED patients compared with AWD patients (Fig. 4L). Conversely, while serum levels of the immunosuppressive M2-cytokine IL-10 were significantly increased in sarcoma patients compared to healthy donors (HD), no significant differences were found between NED and AWD patients. Collectively, these findings underscore the critical role of Th1/Th2 immune balance in modulating stem cell phenotype and disease progression. Consistently, a comparable Th1/Th2 cytokine profile was also detected in melanoma patients, highlighting the critical influence of Th1/Th2 immune polarization in modulating the clinical trajectory of the disease (Supplementary Fig. S5E). Further stratification of sarcoma patients based on IFNγ expression revealed that high IFNγ levels inversely correlated with *SOX2* expression (Fig. 4M), indicative of reduced stemness, and with lower *ZEB1* expression (Fig. 4N), suggestive of diminished EMT potential. Correlation analysis confirmed a robust anti-correlation (Spearman correlation coefficient = -0.329, p-value = 7.03e(-08)) between the Th1 signature and EMT-related *ZEB1* gene expression across the cohort (Fig. 4O). Importantly, a similar pattern was observed in melanoma patients, where elevated IFNγ levels were associated with decreased *NANOG* expression (Supplementary Fig. S5F), indicating that Th1-driven suppression of CSC traits is conserved across tumor types. Collectively, these analyses demonstrate that a Th1-dominant immune milieu, characterized by elevated IFNγ, is associated with the concomitant inhibition of CSC and EMT programs and predicts favorable clinical outcomes, highlighting the translational significance of Th1-mediated immune modulation.

Downloaded from aacrjournals.org/cancerimmunolres/article-pdf/doi/10.1158/2326-6066.CIR-26-0211/3849116/cir-26-0211.pdf by guest on 22 November 2026

Th1/Th2 balance regulates CSC drug resistance.

CSC are thought to be responsible for chemoresistance and cancer recurrence, as they have the ability to self-renew and differentiate into heterogeneous tumor lineages in response to chemotherapy [12]. This resistance is largely due to the mechanisms of action of conventional chemotherapy, including doxorubicin (DOXO) which targets rapidly dividing cells and acts in a cell cycle-specific manner [35–37]. Based on our results, we therefore hypothesized that combining IFNγ (20 ng/ml) with DOXO could increase the chemotherapeutic efficacy, reducing drug resistance, while an opposite effect was expected with cotreatment with IL-4.

To this aim, fibrosarcoma MN/MCA-1 cells were grown under specific spheroid culture conditions in the presence of different concentrations of IFNγ (20 ng/ml or 0,2 ng/ml) or IL-4 (20 ng/ml) for 72h and then treated with DOXO (0,7 μM) for 48h. As demonstrated in Fig. 5A-B, high-dose IFNγ treatment (20 ng/ml) reduced spheroid formation (Fig. 5A, top) and spheroid diameter (Fig. 5A, bottom, left) and enhanced both DOXO-induced CSC death (Fig. 5B) and DOXO-mediated reduction in spheroid diameter (Fig. 5A, bottom, right). Accordingly, the Annexin V-PI assay used to estimate the extent of apoptosis confirmed that combined treatment with high IFNγ (20 ng/ml) and DOXO significantly increased the percentage of early apoptotic cells (Fig. 5C). In contrast, consistent with the observed promotion of the CSC phenotype, IL-4 or low concentrations of IFNγ (0,2 ng/ml) significantly attenuated the effects of DOXO on reducing spheroid diameter and inducing cell death (Fig. 5A-C).

The known mutual antagonism between IFNγ and IL-4 [38] was confirmed using high doses of IFNγ (20 ng/ml), which inhibited the IL-4-mediated increase in spheroid diameter and the rate-limiting effect exerted by IL-4 on DOXO cytotoxicity (Fig. 5A-C). These results suggest that, within the TME, the balance between Th1 and Th2 polarizing signals regulates CSC survival and stemness in a dose-dependent manner. Indeed, no significant influence of low-dose of IFNγ on IL-4 activity was detected (Fig. 5A-C).

Downloaded from aacrjournals.org/cancerimmunolres/article-pdf/doi/10.1158/2326-6066.CIR-26-0211/3849116/cir-26-0211.pdf by guest on 22 November 2026

To further validate these findings, we performed analogous *in vitro* experiments using YUMM1.7 melanoma cells, which harbor the $BRAF^{V600E}$ mutation [39]. Cells were cultured under spheroid-promoting conditions and treated with IL-4 (20 ng/ml), high-dose IFNγ (20 ng/ml), low-dose IFNγ (0,2 ng/ml) or their combination for 1 week, followed by treatment with a BRAF inhibitor (PLX4032, 10 μM) [40]. Consistent with the fibrosarcoma model, high-dose IFNγ treatment impaired spheroid formation and enhanced PLX4032 cytotoxicity, as evidenced by reduced spheroid diameter and increased apoptotic cell death (Supplementary Fig. S6A-B). Conversely, IL-4 and low-dose IFNγ promoted a stem-like (Supplementary Fig. S6A), therapy-resistant phenotype, reducing sensitivity to BRAF inhibition (Supplementary Fig. S6A-B). Notably, co-treatment with high-dose IFNγ was able to reverse IL-4–mediated effects, restoring drug sensitivity and reducing spheroid viability (Supplementary Fig. S6A-B). These data further support the notion that the Th1/Th2 cytokine balance plays a pivotal role in modulating the CSC phenotype and therapeutic response across distinct tumor types.

ATP-binding cassette (ABC) superfamily transporters are considered mediators of multidrug resistance (MDR) in cancer [41], where the efflux of chemotherapeutic drugs causes a reduction in therapeutic efficacy. Since DOXO is a substrate of both the multi-drug resistance protein 1 (MDR1) and the ABC-subfamily G member 2 (ABCG2) [42], we evaluated the putative effects of treatment with IFNγ (20 ng/ml or 0,2 ng/ml) and IL-4 (20 ng/ml) on *MDR1* and *ABCG2* gene expression in fibrosarcoma cells grown under specific spheroid culture conditions. In line with our previous observations, we observed that 72h of treatment with high-dose IFNγ significantly reduced *MDR1* and *ABCG2* expression while IL-4 and low-dose IFNγ increased the expression of both ABC transporters, as compared to untreated cells (Fig. 5D). Notably, treatment with DOXO alone did not alter MDR*1* and *ABCG2* expression.

Having demonstrated the modulation of MDR1 and ABCG2 expression by IFNγ and IL-4, we then determined whether these effects correlated with a differences in the intracellular accumulation of DOXO in CSC. To this end, flow cytometry quantification of intracellular DOXO fluorescence was

Downloaded from aacrjournals.org/cancerimmunolres/article-pdf/doi/10.1158/2326-6066.CIR-26-0211/3849116/cir-26-0211.pdf by guest on 22 November 2026

performed at different time points in the fibrosarcoma MN/MCA-1-derived CSC, treated or not with IFNγ or IL-4. In line with the modulation of ABC transporter genes, we observed that the mean intracellular fluorescence intensity (MFI) of DOXO, assessed after 24h of DOXO treatment, was significantly lower in cells treated with either IL-4 or a low concentration of IFNγ, compared to cells treated with DOXO alone, thus supporting the increased resistance of these cells to DOXO treatment via increased drug extrusion (Fig. 5E). Conversely, treatment with a high concentration of IFNγ increased the intracellular MFI of DOXO, suggesting that the reduced extrusion of DOXO (Fig. 5E) supports the increased cytotoxicity of DOXO under these conditions.

Dose-dependent IFNγ signaling events control CSC fate.

Confirming the role of p50 NF-κB in modulating functional states of the immune compartment associated with tumor CSC development and resistance to chemotherapy, we observed that DOXO treatment in $p50^{fl/fl}$*Tie2-Cre* fibrosarcoma-bearing mice significantly reduced lung metastasis formation compared with in $p50^{fl/fl}$ tumor-bearing mice (Fig. 5F).

To mechanistically dissect the dose-dependent effects of IFNγ, we investigated its canonical downstream signaling pathways. Consistent with previous findings in NSCLC [43], exposure of fibrosarcoma spheroids to high-dose IFNγ (20 ng/ml) led to strong activation of the JAK1-STAT1 axis, evidenced by increased STAT1 expression and phosphorylation (Fig. 6A) and subsequent induction of pro-apoptotic programs characterized by caspase-3 cleavage [44]. By contrast, low-dose IFNγ (0.2 ng/ml) preferentially activated the PI3K/AKT pathway, as attested by enhanced AKT phosphorylation, thereby promoting metabolic adaptation, survival and multidrug resistance [45] (Fig. 6A). Given the striking phenotypic similarities between IL-4 treatment and low-dose IFNγ observed throughout the study, we next explored the signaling pathways activated by IL-4 in tumor cells (Supplementary Fig. S6C). As expected, IL-4 activated the canonical STAT6 signaling pathway, as evidenced by increased STAT6 phosphorylation. In parallel, IL-4 also enhanced AKT phosphorylation (Supplementary Fig. S6C), indicating concomitant activation of the PI3K/AKT

Downloaded from aacrjournals.org/cancerimmunolres/article-pdf/doi/10.1158/2326-6066.CIR-26-0211/3849116/cir-26-0211.pdf by guest on 22 November 2026

pathway. These findings provide a mechanistic explanation for the comparable effects elicited by IL-4 and low-dose IFNγ on CSC expansion, spheroid growth and chemoresistance (Fig. 5 and Supplementary Fig. S6A-B), suggesting that, despite engaging distinct upstream receptors, IL-4 and low-dose IFNγ converge on PI3K/AKT signaling to sustain stem-like and drug-resistant phenotypes.

Pharmacological modulation confirmed the functional relevance of these pathways. Treatment of fibrosarcoma spheroids with Ruxolitinib (RX), a clinically approved JAK1/2 inhibitor [46], completely abrogated the reduction in spheroid diameter (Fig. 6B) induced by high-dose IFNγ, underscoring the requirement of intact JAK/STAT1 signaling for the suppression of CSC proliferation. Conversely, blockade of the PI3K/AKT axis with PF-04691502 (PF) [47] significantly impaired the stemness-promoting and chemoprotective effects of low-dose IFNγ, restoring spheroid shrinkage to levels comparable to untreated controls (Fig. 6B).

When combined with DOXO, pathway-specific inhibition functionally reverted IFNγ-mediated phenotypes. As shown in Fig. 6C, blockade of JAK1/2 with RX prevented the chemosensitizing activity of high-dose IFNγ, restoring spheroid diameter to levels comparable to DOXO alone. Conversely, inhibition of PI3K/AKT with PF abrogated the cytoprotective effect of low-dose IFNγ, re-establishing spheroid shrinkage in response to DOXO. Consistently, Annexin V/PI assays (Fig. 6D) demonstrated that the pro-apoptotic effect elicited by high-dose IFNγ was lost upon JAK1/2 inhibition, whereas the survival advantage conferred by low-dose IFNγ was reversed by PI3K/AKT blockade. In particular, the pronounced increase in apoptotic populations induced by high-dose IFNγ in combination with DOXO was completely abrogated upon JAK1/2 blockade with RX, mirroring the loss of its chemosensitizing activity (Fig. 6D, right); conversely, PI3K/AKT inhibition with PF selectively neutralized the survival-promoting effect of low-dose IFNγ, as evidenced by a marked increase in of early- and late-apoptotic fractions comparable to DOXO treatment alone (Fig. 6D, right). Together, these findings delineate a dose-dependent molecular switch: while high-dose IFNγ engages the JAK1–STAT1–caspase axis to drive apoptosis and chemosensitization, low-dose

Downloaded from aacrjournals.org/cancerimmunolres/article-pdf/doi/10.1158/2326-6066.CIR-26-0211/3849116/cir-26-0211.pdf by guest on 22 November 2026

IFNγ co-opts PI3K/AKT signaling to reinforce stem-like, drug-resistant phenotypes. Importantly, IL-4 activates both the canonical STAT6 pathway and PI3K/AKT signaling, providing a mechanistic basis for the functional overlap observed between IL-4 and low-dose IFNγ in sustaining CSC maintenance and chemoresistance-associated phenotypes. From a translational perspective, this dualism highlights that preserving STAT1 activity is critical for leveraging IFNγ-based therapies, whereas selective targeting of PI3K/AKT signaling may provide a strategy to overcome chemoresistance and stemness driven by low IFNγ signaling in the TME.

The IFNγ-dependent Th1/Th2 balance regulates the efficacy of therapy in vivo.

Failure of IFNγ signaling has been identified as a mechanism of resistance to checkpoint blockade in solid tumors, and IFNγ activity is considered necessary and prognostic for immunotherapy across multiple cancer types [48]. Moreover, the combination of immune checkpoint inhibitors (ICIs) with chemotherapy may lead to improved responses even in tumor types insensitive to ICB monotherapy [49]. Based on this, as well as on the observation that $p50^{fl/fl}$*Tie2-Cre* fibrosarcoma-bearing mice display increased IFNγ expression by both $CD4^+$ and $CD8^+$ T cells (Fig. 3J), we tested whether blocking IFNγ activity could influence ICI-based immunotherapy or chemotherapy in MN/MCA-1-bearing mice.

To this aim, WT mice injected with MN/MCA-1 cells were first treated with either an αPD-1 antibody alone or αPD-1 plus αIFNγ. Compared with mice that received vehicle alone, αPD-1 treatment reduced primary tumor growth (Fig. 7A) and increased IFNγ production by $CD4^+$ and $CD8^+$ cells (Fig. 7B). Moreover, consistent with the anti-CSC effect exerted by high doses of IFNγ on tumor cells, αPD-1-treated mice presented a lower frequency of c-kit^+ CSC (Fig. 7C, left), which displayed a prominent epithelial phenotype, as indicated by higher expression of E-cadherin (Fig. 7C, right), in parallel with a reduced number of lung metastases (Fig. 7D). Remarkably, concomitant treatment with αIFNγ completely abolished all these αPD-1-elicited effects (Fig. 7A-

Downloaded from aacrjournals.org/cancerimmunolres/article-pdf/doi/10.1158/2326-6066.CIR-26-0211/3849116/cir-26-0211.pdf by guest on 22 November 2026

D), supporting the hypothesis that a Th1 response, primarily mediated by IFNγ, impairs the aggressive CSC phenotype. Similarly, αPD-1 treatment in B16/F10 melanoma-bearing mice led to a significant reduction in primary tumor growth (Supplementary Fig. S6D) and increased IFNγ production by both $CD4^+$ and $CD8^+$ T cells (Supplementary Fig. S6E), accompanied by a decrease in the frequency of $CD20^+$ tumor cells and an increase in the epithelial phenotype, as evidenced by the high expression of E-cadherin (Supplementary Fig. S6D). Notably, co-administration of αIFNγ completely abolished the therapeutic effects of αPD-1, further highlighting the pivotal role of IFNγ in modulating the CSC phenotype. Likewise, co-treatment of fibrosarcoma-bearing WT mice with αPD-1 (Fig. 7E, left) or a high dose IFNγ (1 μg/mice, Fig. 7E, right) enhanced the antitumor efficacy of DOXO, as evidenced by a further reduction in primary tumor volume and the number of lung metastases, while the capacity of either αPD-1 or IFNγ to enhance DOXO-mediated antitumor activity was lost when mice were also treated with αIFNγ (Fig. 7E). Consistent with our *in vitro* findings showing that low doses of IFNγ promote stem-like properties, *in vivo* administration of low doses of IFNγ (0.1 or 0.01 μg/mouse) in combination with DOXO in MN/MCA-1-bearing mice resulted in a significant loss of chemotherapy-induced cytotoxicity and a paradoxical increase in lung metastases formation (Fig. 7F). These results support the notion that low-dose IFNγ signaling fosters a pro-stemness and therapy-resistant tumor phenotype, compromising the effectiveness of the treatment. Notably, when the IFNγ dose was further reduced to 0.001 μg/mouse, its pro-stemness and pro-metastatic effects were lost, suggesting that a finely tuned balance of IFNγ concentrations within the tumor microenvironment crucially controls tumor cell plasticity and response to therapy. Confirming the relevance of Th1/Th2 balance in orchestrating both the CSC phenotype and clinical response, blockade of the prototypical Th2 cytokine IL-4 by administration of an α-IL-4 antibody in MN/MCA-1-bearing mice resulted in reduced lung metastasis formation (Fig. 7G), as well as in the enhancement of the antitumor response to both DOXO and Th1-polarizing treatments (IFNγ or αPD-1) (Fig. 7G).

Downloaded from aacrjournals.org/cancerimmunolres/article-pdf/doi/10.1158/2326-6066.CIR-26-0211/3849116/cir-26-0211.pdf by guest on 22 November 2026

Consistent with these findings, in the melanoma model, combination treatments targeting either the enhancement of Th1 responses (via IFNγ or αPD-1) or the blockade of Th2 signaling (via αIL-4) resulted in a greater antitumor activity compared with the respective single treatments (Supplementary Fig. S6F). Overall, these findings underscore the centrality of the Th1/Th2 balance in regulating tumor cell stemness and response to therapies, supporting the idea that strategies that promote a Th1 immune profile in patients may have beneficial effects on clinical outcome in response to chemotherapy and immunotherapy.

DISCUSSION

Our study delineates the Th1/Th2 balance as a central determinant of tumor progression, CSC maintenance, and therapeutic response. Specifically, we demonstrate that reprogramming the tumor immune microenvironment toward an M1/Th1-dominant state, associated with enhanced IFNγ-producing T-cell responses, limits CSC survival and increases chemosensitivity. Consistently, a Th2/IL-4 dominant immune profile, or suboptimal IFNγ signaling, promotes CSC persistence and resistance to therapy, offering a further mechanistic interpretation of the prognostic validity of the "immunoscore classification" [2], as well as of the poor therapeutic response typical of immunologically "cold" tumors [50]. In addition to confirming the need for enhanced IFNγ signaling for an effective antitumor response [51], our study further demonstrates that the Th1/Th2 balance, as well as IFNγ levels, is a key regulator of CSC plasticity, expanding our understanding of the mechanisms underlying treatment responses [52,53]. Indeed, our data highlight that, in addition to intrinsic tumor heterogeneity caused by genomic instability, the TME immunoprofile acts as a major Darwinian selective force for therapy-refractory CSC, sculpting tumor cell traits that promote survival, immune evasion and CSC plasticity [54]. Within this framework, the immunoprofile of the TME, including the expression of immune checkpoints, emerges not only as a prognostic marker but also as an active determinant of disease trajectory [55]. Our findings further refine this concept, strengthening the idea that key transcriptional regulators of immune polarization (i.e., p50 NF-κB)

Downloaded from aacrjournals.org/cancerimmunolres/article-pdf/doi/10.1158/2326-6066.CIR-26-0211/3849116/cir-26-0211.pdf by guest on 22 November 2026

govern tumor selection and heterogeneity. While several innate and adaptive immune populations were remodeled in p50-deficient tumors, our functional studies specifically identify Th1-polarized $CD4^+$ T cells as a major immune population contributing to CSC control. These findings should, however, be interpreted within the broader role of p50 NF-κB as a central regulator of tumor immune polarization. As previously shown by our group, p50 deficiency reprograms TAMs and $Ly6C^{hi}$ monocytes from an immunosuppressive to a pro-inflammatory phenotype, thereby relieving myeloid-mediated immune suppression and promoting Th1 immunity [5, 6] . Consistent with these observations, p50-deficient tumors displayed reduced accumulation of TAMs, expansion of inflammatory $Ly6C^{hi}$ monocytes, acquisition of an M1-like macrophage phenotype, increased infiltration of NK and NKT cells and enhanced IFNγ production by both $CD4^+$ and $CD8^+$ T cells . Collectively, these findings support a model in which p50 NF-κB orchestrates the establishment of a multicellular Th1-polarized tumor microenvironment that enables $CD4^+$ Th1 cells to exert their antitumor and anti-CSC activity.

In this context, our data are consistent with a hierarchical rather than cell-restricted model linking hematopoietic p50 deficiency to CSC regulation. Loss of p50 broadly remodels the tumor immune compartment, including attenuation of myeloid immunosuppression and activation of lymphoid effector responses. Within this remodeled environment, however, $CD4^+$ T-cell polarization emerges as a major functional downstream axis controlling CSC plasticity. This interpretation is supported by the ability of $CD4^+$ T cells from $p50^{fl/fl}$Tie2-Cre mice, as well as independently polarized Th1 cells, to directly restrain CSC properties, and by the reversal of the anti-CSC phenotype following $CD4^+$ T-cell depletion in vivo. Thus, rather than excluding contributions from other p50-dependent immune populations, we propose that myeloid reprogramming and reduced immunosuppression create permissive conditions for a Th1-dominant response, whose effector cytokines directly influence tumor-cell state. Within this framework, CSC should not be viewed as a fixed tumor cell population but rather as a highly plastic compartment whose maintenance and therapeutic vulnerability are profoundly influenced by the immune landscape. [11]. Despite representing only a

Downloaded from aacrjournals.org/cancerimmunolres/article-pdf/doi/10.1158/2326-6066.CIR-26-0211/3849116/cir-26-0211.pdf by guest on 22 November 2026

minor, immune-privileged fraction of the tumor mass, CSC are intrinsically resistant to conventional therapies and are thought to drive tumor recurrence [13].

Mounting evidence underscores a reciprocal and nuanced interplay between CSC and immune cells, with immune-derived cues shaping CSC biology and CSC, in turn, modulating immune responses [56]. Our study shows that Th1-skewed immune contexts characterized by robust IFNγ signaling suppress CSC programs, whereas Th2-biased/IL-4 or suboptimal IFNγ signaling supports CSC survival and expansion. The observation that IL-4 elicited CSC-related phenotypes similar to those induced by low-dose IFNγ, together with its ability to activate STAT6 and PI3K/AKT signaling, further supports the existence of shared downstream signaling pathways regulating CSC plasticity within an immunosuppressive TME.

Although IL-6 has frequently been implicated in promoting EMT and CSC maintenance, our findings indicate that its biological effects are highly context-dependent and should be interpreted within the overall immune milieu; in our model, elevated IL-6 levels were associated with a strongly Th1-polarized tumor microenvironment characterized by high IFNγ and reduced IL-4, in which CSC frequency, stemness and metastatic potential were markedly reduced. These observations suggest that, in this setting, the antitumor activity associated with a robust Th1 immune response overrides the protumorigenic effects that have been attributed to IL-6 in other contexts. Overall, the Th1/Th2 immune balance, rather than the level of an individual cytokine, is the major determinant of CSC plasticity.

These findings are consistent with prior reports underscoring the dual, context-dependent role of IFNγ in tumor biology [57–59]. High-dose or acute IFNγ activates apoptotic pathways in cancer cells through the JAK/STAT1/STAT4 axis, induces MHC-I expression, recruits cytotoxic $CD8^+$ T cells and polarizes macrophages toward a pro-inflammatory phenotype, collectively promoting tumor rejection [60–62]. Conversely, low-dose or suboptimal IFNγ signaling paradoxically enhances CSC traits, EMT, metastasis and immune evasion by upregulating PD-L1 and IDO1, with potent immunosuppressive effects [58,63–66].

Downloaded from aacrjournals.org/cancerimmunolres/article-pdf/doi/10.1158/2326-6066.CIR-26-0211/3849116/cir-26-0211.pdf by guest on 22 November 2026

Importantly, the high- and low-dose IFNγ conditions used here should not be interpreted as direct quantitative surrogates of IFNγ concentrations within the TME. Our flow-cytometric analyses demonstrate increased IFNγ-producing capacity of tumor-infiltrating T cells in $p50^{fl/fl}$Tie2-Cre mice, but do not measure the local concentration of bioavailable IFNγ to which individual tumor cells are exposed. Rather, the two in vitro concentrations identify distinct signaling regimes, indicating that the biological outcome of IFNγ exposure critically depends on signal strength. This distinction may be particularly relevant during immunotherapy, where the magnitude, duration and spatial distribution of IFNγ signaling are likely to be heterogeneous. In NSCLC, low-dose IFNγ is reported to drive CSC phenotypes via ICAM1–PI3K–Akt–Notch1 signaling, whereas high-dose IFNγ promotes apoptosis through JAK1–STAT1–caspase activation [63]. Similarly, in breast cancer Benci et al. highlighted that suboptimal IFNγ signaling promotes immunoediting in favor of CSC, accelerating disease progression and resistance to immunotherapies [67]. These findings may also have implications for immunotherapy, suggesting that therapeutic efficacy may depend not simply on the induction of an IFNγ response, but also on the magnitude of IFNγ signaling within the TME, with robust signaling favoring antitumor and anti-stemness activity, whereas suboptimal signaling may instead support therapy-resistant CSC states.

These studies are consistent with our observations, supporting the existence of a dual-function switch for IFNγ, capable of altering the balance between tumor suppression and CSC promotion in a dose-dependent manner. Indeed, we observed that high-dose IFNγ (20 ng/ml) favors the activation of the pro-apoptotic JAK1-STAT1 axis, while low-dose IFNγ (0.2 ng/ml) preferentially promotes the pro-survival PI3K/AKT pathway, supporting chemotherapy resistance. This observation underscores the importance of the intensity of immune responses and signaling thresholds in determining therapeutic outcomes and is consistent with previous observations on the dual nature of IFNγ, showing that elevated IFNγ gene signatures correlate with favorable responses to immune checkpoint inhibitor therapy, including anti-PD-1/PD-L1 agents, and are associated with enhanced Th1 immunity and cytotoxic T cell activity [68].

Downloaded from aacrjournals.org/cancerimmunolres/article-pdf/doi/10.1158/2326-6066.CIR-26-0211/3849116/cir-26-0211.pdf by guest on 22 November 2026

Conversely, chronic exposure to IFNγ or the simultaneous activation of immunosuppressive mechanisms, such as IDO1 induction and Treg expansion, may promote resistance to ICIs [69–73]. Together with our findings showing that suboptimal IFNγ signaling compromises chemotherapy efficacy and promotes therapy-resistant CSC phenotypes, these observations suggest that not only the presence but also the magnitude and duration of IFNγ signaling may critically influence therapeutic outcomes. Importantly, our clinical analyses are consistent with this model, as sarcoma and melanoma patients with a favorable prognosis displayed higher systemic levels of Th1-associated immune mediators, whereas transcriptomic analyses across independent human sarcoma and melanoma cohorts demonstrated that a robust Th1 immune signature strongly correlates with improved clinical outcomes. These findings support the concept that the quality, intensity and persistence of the Th1 immune response, rather than IFNγ expression alone, are critical determinants of tumor evolution and therapeutic responsiveness. Accordingly, IFNγ should not be regarded as a binary biomarker, but rather as a context-dependent signal whose biological effects are shaped by both its concentration and the surrounding immune landscape. Therefore, stratification according to intratumoral IFNγ levels or, more broadly, a Th1-oriented immune signature may help identify patients more likely to benefit from therapies that reinforce a productive Th1 immune response while avoiding potentially ineffective or even detrimental interventions in tumors dominated by chronic, suboptimal IFNγ signaling. Although the predictive value of intratumoral IFNγ activity and Th1 signatures for treatment response warrants prospective validation in clinically annotated cohorts, our findings provide a strong rationale for incorporating quantitative immune profiling into future clinical trial design. Future clinical trials should therefore integrate longitudinal assessment of intratumoral IFNγ activity together with broader Th1-associated immune signatures to determine whether the intensity and persistence of IFNγ signaling predict treatment efficacy or resistance.

Crucially our study adds insights by demonstrating that modulation of the Th1/Th2 cytokine axis via NF-κB p50–dependent immune polarization can reprogram the TME to suppress CSC programs

Downloaded from aacrjournals.org/cancerimmunolres/article-pdf/doi/10.1158/2326-6066.CIR-26-0211/3849116/cir-26-0211.pdf by guest on 22 November 2026

and enhance chemosensitivity, linking immune polarization, interferon signaling and CSC-mediated treatment outcomes.

Overall, our findings support a model in which therapy resistance is regulated by the polarization and intensity of the immune response, reaffirming the Th1/Th2 balance as a key determinant of tumor evolution. From a translational perspective, our data suggest that therapeutic strategies should aim to promote a coordinated Th1-polarized immune response rather than simply increase IFNγ levels, as suboptimal IFNγ signaling may paradoxically promote CSC maintenance and therapeutic resistance. Accordingly, our findings provide a rationale for combining current immuno- and chemotherapies with interventions that reinforce Th1 polarization or counteract Th2 signaling, thereby limiting CSC plasticity and potentially improving treatment efficacy.

DISCLOSURE OF POTENTIAL CONFLICTS OF INTEREST

The authors declare that the research was conducted in the absence of any commercial or financial relationships that could be construed as a potential conflict of interest.

AUTHORS' CONTRIBUTIONS

FM. Consonni: conceptualization, formal analysis, investigation, methodology, visualization, writing–original draft. **A. Pastò**: conceptualization, formal analysis, investigation, methodology, writing–original draft. **G. Ballerini**: formal analysis, investigation, methodology. **M. Storto**: investigation, methodology. **F. Guana**: formal analysis, methodology. **M. Incerti**: methodology. **M. Sironi**: methodology. **P. Ostano**: formal analysis. **G. Chiorino**: formal analysis, methodology. **A. Amadori**: conceptualization. **A. Sica**: conceptualization, supervision, methodology, funding acquisition, writing–original draft.

Downloaded from aacrjournals.org/cancerimmunolres/article-pdf/doi/10.1158/2326-6066.CIR-26-0211/3849116/cir-26-0211.pdf by guest on 22 November 2026

REFERENCES

1. Pagès F, Galon J, Dieu-Nosjean MC, Tartour E, Sautès-Fridman C, Fridman WH. Immune infiltration in human tumors: A prognostic factor that should not be ignored. Oncogene. 2010. p. 1093–102.
2. Bruni D, Angell HK, Galon J. The immune contexture and Immunoscore in cancer prognosis and therapeutic efficacy. Nat. Rev. Cancer. 2020.
3. Akkari L, Amit I, Bronte V, Fridlender ZG, Gabrilovich DI, Ginhoux F, et al. Defining myeloid-derived suppressor cells. Nat Rev Immunol. 2024;24:850–7.
4. Strauss L, Guarneri V, Gennari A, Sica A. Implications of metabolism-driven myeloid dysfunctions in cancer therapy. Cell. Mol. Immunol. 2021.
5. Mantovani A, Allavena P, Marchesi F, Garlanda C. Macrophages as tools and targets in cancer therapy. Nat. Rev. Drug Discov. 2022. p. 799–820.
6. Saccani A, Schioppa T, Porta C, Biswas SK, Nebuloni M, Vago L, et al. p50 nuclear factor-κB overexpression in tumor-associated macrophages inhibits M1 inflammatory responses and antitumor resistance. Cancer Res. 2006;66:11432–40.
7. Porta C, Consonni FM, Morlacchi S, Sangaletti S, Bleve A, Totaro MG, et al. Tumor-derived prostaglandin E2 promotes p50 NF-kB-dependent differentiation of monocytic MDSCs. Cancer Res. 2020;80:2874–88.
8. Consonni FM, Bleve A, Totaro MG, Storto M, Kunderfranco P, Termanini A, et al. Heme catabolism by tumor-associated macrophages controls metastasis formation. Nat Immunol. 2021;
9. Solis-Castillo LA, Garcia-Romo GS, Diaz-Rodriguez A, Reyes-Hernandez D, Tellez-Rivera E, Rosales-Garcia VH, et al. Tumor-infiltrating regulatory T cells, CD8/Treg ratio, and cancer stem cells are correlated with lymph node metastasis in patients with early breast cancer. Breast Cancer. 2020;27:837–49.
10. Lim B, Woodward WA, Wang X, Reuben JM, Ueno NT. Inflammatory breast cancer biology: the tumour microenvironment is key. Nat. Rev. Cancer. 2018. p. 485–99.
11. Clara JA, Monge C, Yang Y, Takebe N. Targeting signalling pathways and the immune microenvironment of cancer stem cells — a clinical update. Nat. Rev. Clin. Oncol. 2020. p. 204–32.
12. Chu X, Tian W, Ning J, Xiao G, Zhou Y, Wang Z, et al. Cancer stem cells: advances in knowledge and implications for cancer therapy. Signal Transduct. Target. Ther. 2024.
13. Long V. Nguyen, Robert Vanner, Peter Dirks, Connie J. Eaves. Cancer stem cells: an evolving concept. Nat Rev Cancer. 2012;2:133–43.
14. El-Tanani M, Rabbani SA, Satyam SM, Rangraze IR, Wali AF, El-Tanani Y, et al. Deciphering the Role of Cancer Stem Cells: Drivers of Tumor Evolution, Therapeutic Resistance, and Precision Medicine Strategies. Cancers (Basel). 2025.
15. Loret N, Denys H, Tummers P, Berx G. The role of epithelial-to-mesenchymal plasticity in ovarian cancer progression and therapy resistance. Cancers (Basel). 2019.
16. Lei ZN, Teng QX, Koya J, Liu Y, Chen Z, Zeng L, et al. The correlation between cancer stem cells and epithelial-mesenchymal transition: molecular mechanisms and significance in cancer theragnosis. Front. Immunol. 2024.
17. Mantovani A, Marchesi F, Di Mitri D, Garlanda C. Macrophage diversity in cancer dissemination and metastasis. Cell. Mol. Immunol. 2024. p. 1201–14.
18. Bied M, Ho WW, Ginhoux F, Blériot C. Roles of macrophages in tumor development: a spatiotemporal perspective. Cell. Mol. Immunol. 2023. p. 983–92.
19. Plaks V, Kong N, Werb Z. The cancer stem cell niche: How essential is the niche in regulating stemness of tumor cells? Cell Stem Cell. 2015. p. 225–38.
20. Hsu YC, Fuchs E. A family business: Stem cell progeny join the niche to regulate homeostasis.

Downloaded from aacrjournals.org/cancerimmunolres/article-pdf/doi/10.1158/2326-6066.CIR-26-0211/3849116/cir-26-0211.pdf by guest on 22 November 2026

Nat. Rev. Mol. Cell Biol. 2012. p. 103–14.
21. Liguori M, Digifico E, Vacchini A, Avigni R, Colombo FS, Borroni EM, et al. The soluble glycoprotein NMB (GPNMB) produced by macrophages induces cancer stemness and metastasis via CD44 and IL-33. Cell Mol Immunol. 2021;18:711–22.
22. Jinushi M, Chiba S, Yoshiyama H, Masutomi K, Kinoshita I, Dosaka-Akita H, et al. Tumor-associated macrophages regulate tumorigenicity and anticancer drug responses of cancer stem/initiating cells. Proc Natl Acad Sci U S A. 2011;108:12425–30.
23. Verona F, Di Bella S, Schirano R, Manfredi C, Angeloro F, Bozzari G, et al. Cancer stem cells and tumor-associated macrophages as mates in tumor progression: mechanisms of crosstalk and advanced bioinformatic tools to dissect their phenotypes and interaction. Front. Immunol. 2025.
24. Zhang W, Zhou R, Xin LIU, Lin YOU, Chen C, Xiaoling YE, et al. Key role of exosomes derived from M2 macrophages in maintaining cancer cell stemness (Review). Int J Oncol. 2023;63.
25. Etzerodt A, Moulin M, Doktor TK, Delfini M, Mossadegh-Keller N, Bajenoff M, et al. Tissue-resident macrophages in omentum promote metastatic spread of ovarian cancer. J Exp Med. 2020;217.
26. Mantovani A, Marchesi F, Malesci A, Laghi L, Allavena P. Tumour-associated macrophages as treatment targets in oncology. Nat. Rev. Clin. Oncol. 2017. p. 399–416.
27. Foster BM, Zaidi D, Young TR, Mobley ME, Kerr BA. CD117/c-kit in cancer stem cell-mediated progression and therapeutic resistance. Biomedicines. 2018.
28. Liu A, Yu X, Liu S. Pluripotency transcription factors and cancer stem cells: Small genes make a big difference. Chin. J. Cancer. 2013. p. 483–7.
29. Amini S, Fathi F, Mobalegi J, Sofimajidpour H, Ghadimi T. The expressions of stem cell markers: Oct4, Nanog, Sox2, nucleostemin, Bmi, Zfx, Tcl1, Tbx3, Dppa4, and Esrrb in bladder, colon, and prostate cancer, and certain cancer cell lines. Anat Cell Biol. 2014;47:1–11.
30. Porta C, Rimoldi M, Raes G, Brys L, Ghezzi P, Di Liberto D, et al. Tolerance and M2 (alternative) macrophage polarization are related processes orchestrated by p50 nuclear factor κB. Proc Natl Acad Sci U S A. 2009;106:14978–83.
31. Porta C, Ippolito A, Consonni FM, Carraro L, Celesti G, Correale C, et al. Protumor steering of cancer inflammation by p50 nf-kb enhances colorectal cancer progression. Cancer Immunol Res. 2018;
32. Lambert AW, Weinberg RA. Linking EMT programmes to normal and neoplastic epithelial stem cells. Nat Rev Cancer. 2021;21:325–38.
33. Gurram RK, Wei D, Yu Q, Butcher MJ, Chen X, Cui K, et al. Crosstalk between ILC2s and Th2 cells varies among mouse models. Cell Rep. 2023;42.
34. Murphy KM, Reiner SL. The lineage decisions of helper T cells. Nat. Rev. Immunol. 2002. p. 933–44.
35. Mattioli R, Ilari A, Colotti B, Mosca L, Fazi F, Colotti G. Doxorubicin and other anthracyclines in cancers: Activity, chemoresistance and its overcoming. Mol. Aspects Med. 2023.
36. Christowitz C, Davis T, Isaacs A, Van Niekerk G, Hattingh S, Engelbrecht AM. Mechanisms of doxorubicin-induced drug resistance and drug resistant tumour growth in a murine breast tumour model. BMC Cancer. 2019;19.
37. Kar A, Agarwal S, Singh A, Bajaj A, Dasgupta U. Insights into molecular mechanisms of chemotherapy resistance in cancer. Transl Oncol. 2024;42.
38. Paludan SR. Interleukin-4 and interferon-γ: The quintessence of a mutual antagonistic relationship. Scand. J. Immunol. 1998. p. 459–68.
39. Meeth K, Wang JX, Micevic G, Damsky W, Bosenberg MW. The YUMM lines: a series of congenic mouse melanoma cell lines with defined genetic alterations. Pigment Cell Melanoma Res. 2016;29:590–7.
40. Joseph EW, Pratilas CA, Poulikakos PI, Tadi M, Wang W, Taylor BS, et al. The RAF inhibitor PLX4032 inhibits ERK signaling and tumor cell proliferation in a V600E BRAF-selective manner. Proc Natl Acad Sci U S A. 2010;107:14903–8.

Downloaded from aacrjournals.org/cancerimmunolres/article-pdf/doi/10.1158/2326-6066.CIR-26-0211/3849116/cir-26-0211.pdf by guest on 22 November 2026

41. Wang JQ, Wu ZX, Yang Y, Teng QX, Li YD, Lei ZN, et al. ATP-binding cassette (ABC) transporters in cancer: A review of recent updates. J. Evid. Based. Med. 2021. p. 232–56.
42. Mirzaei S, Gholami MH, Hashemi F, Zabolian A, Farahani MV, Hushmandi K, et al. Advances in understanding the role of P-gp in doxorubicin resistance: Molecular pathways, therapeutic strategies, and prospects. Drug Discov. Today. 2022. p. 436–55.
43. Song M, Ping Y, Zhang K, Yang L, Li F, Zhang C, et al. Low-dose IFNg induces tumor cell stemness in tumor microenvironment of non–small cell lung cancer. Cancer Res. 2019;79:3737–48.
44. Sironi JJ, Ouchi T. STAT1-induced Apoptosis Is Mediated by Caspases 2, 3, and 7. J Biol Chem. 2004;279:4066–74.
45. Liu R, Chen Y, Liu G, Li C, Song Y, Cao Z, et al. PI3K/AKT pathway as a key link modulates the multidrug resistance of cancers. Cell Death Dis. 2020.
46. Ostojic A, Vrhovac R, Verstovsek S. Ruxolitinib: A new JAK1/2 inhibitor that offers promising options for treatment of myelofibrosis. Futur Oncol. 2011;7:1035–43.
47. Cheng H, Bagrodia S, Bailey S, Edwards M, Hoffman J, Hu Q, et al. Discovery of the highly potent PI3K/mTOR dual inhibitor PF-04691502 through structure based drug design. Medchemcomm. 2010;1:139–44.
48. Paschen A, Melero I, Ribas A. Central Role of the Antigen-Presentation and Interferon-γ Pathways in Resistance to Immune Checkpoint Blockade. Annu. Rev. Cancer Biol. 2022. p. 85–102.
49. Alsaafeen BH, Ali BR, Elkord E. Combinational therapeutic strategies to overcome resistance to immune checkpoint inhibitors. Front. Immunol. 2025.
50. Wu B, Zhang B, Li B, Wu H, Jiang M. Cold and hot tumors: from molecular mechanisms to targeted therapy. Signal Transduct. Target. Ther. 2024.
51. Shankaran V, Ikeda H, Bruce AT, White JM, Swanson PE, Old LJ, et al. Pillars Article: IFNγ and Lymphocytes Prevent Primary Tumour Development and Shape Tumour Immunogenicity. Nature . 2001. 410: 1107–1111. J Immunol. 2018;201:827–31.
52. Espinosa-Carrasco G, Chiu E, Scrivo A, Zumbo P, Dave A, Betel D, et al. Intratumoral immune triads are required for immunotherapy-mediated elimination of solid tumors. Cancer Cell. 2024;42:1202-1216.e8.
53. Jou E. Type 1 and type 2 cytokine-mediated immune orchestration in the tumour microenvironment and their therapeutic potential. Explor. Target. Anti-tumor Ther. 2023. p. 474–97.
54. Khong HT, Restifo NP. Natural selection of tumor variants in the generation of “tumor escape” phenotypes. Nat Immunol. 2002;3:999–1005.
55. Karihtala K, Leivonen SK, Karjalainen-Lindsberg ML, Chan FC, Steidl C, Pellinen T, et al. Checkpoint protein expression in the tumor microenvironment defines the outcome of classical Hodgkin lymphoma patients. Blood Adv. 2022;6:1919–31.
56. Pastò A, Consonni FM, Sica A. Influence of innate immunity on cancer cell stemness. Int. J. Mol. Sci. 2020.
57. Liu X. The paradoxical role of IFN-γ in cancer: Balancing immune activation and immune evasion. Pathol. Res. Pract. 2025. p. 156046.
58. Gocher AM, Workman CJ, Vignali DAA. Interferon-γ: teammate or opponent in the tumour microenvironment? Nat. Rev. Immunol. 2022. p. 158–72.
59. Galassi C, Galluzzi L. Cancer stem cell immunoediting by IFNγ. Cell Death Dis. 2023.
60. Zhang Y, Khanniche A, Li Y, Wu Z, Wang H, Zhang H, et al. A myeloid IFN gamma response gene signature correlates with cancer prognosis. Clin Transl Med. 2025;15.
61. Yuan F, Wang L, Ning L, Zhang J, Guo Y. Gas-mediated reinforcement of cancer therapies: emerging strategies and future perspectives. Chem Sci. 2025;16:20108–23.
62. Gao AH, Hu YR, Zhu WP. IFN-γ inhibits ovarian cancer progression via SOCS1/JAK/STAT signaling pathway. Clin Transl Oncol. 2022;24:57–65.
63. Song M, Ping Y, Zhang K, Yang L, Li F, Research CZ-C, et al. Low-Dose IFNγ Induces Tumor

Downloaded from aacrjournals.org/cancerimmunolres/article-pdf/doi/10.1158/2326-6066.CIR-26-0211/3849116/cir-26-0211.pdf by guest on 22 November 2026

Cell Stemness in Tumor Microenvironment of Non-Small Cell Lung Cancer. Cancer Res [Internet]. 2019; Available from: https://aacrjournals.org/cancerres/article-abstract/79/14/3737/638366
64. Zhao W, Wang H, Zhang X, Zhang L, Pu W, Ma Y, et al. Effects of IFN-γ on the immunological microenvironment and TAM polarity in stage IA non-small cell lung cancer and its mechanisms. BMC Pulm Med. 2024;24.
65. Snyder M, Wang Z, Lara B, Fimbres J, Pichardo T, Mazzilli S, et al. The aryl hydrocarbon receptor controls IFN-γ-induced immune checkpoints PD-L1 and IDO via the JAK/STAT pathway in lung adenocarcinoma. J Immunol. 2025;214:413–32.
66. He YF, Wang XH, Zhang GM, Chen HT, Zhang H, Feng ZH. Sustained low-level expression of interferon-γ promotes tumor development: Potential insights in tumor prevention and tumor immunotherapy. Cancer Immunol Immunother. 2005;54:891–7.
67. Beziaud L, Young CM, Alonso AM, Norkin M, Minafra AR, Huelsken J. IFNγ-induced stem-like state of cancer cells as a driver of metastatic progression following immunotherapy. Cell Stem Cell. 2023;30:818-831.e6.
68. Grasso CS, Tsoi J, Onyshchenko M, Abril-Rodriguez G, Ross-Macdonald P, Wind-Rotolo M, et al. Conserved Interferon-γ Signaling Drives Clinical Response to Immune Checkpoint Blockade Therapy in Melanoma. Cancer Cell. 2020;38:500-515.e3.
69. Ayers M, Lunceford J, Nebozhyn M, Murphy E, Loboda A, Kaufman DR, et al. IFN-γ-related mRNA profile predicts clinical response to PD-1 blockade. J Clin Invest. 2017;127:2930–40.
70. Li S, Li K, Tian F, Li H, Xia Q, Li T, et al. A high interferon gamma signature of CD8+ T cells predicts response to neoadjuvant immunotherapy plus chemotherapy in gastric cancer. Front Immunol. 2023;13.
71. Sceneay J, Goreczny GJ, Wilson K, Morrow S, Decristo MJ, Ubellacker JM, et al. Interferon signaling is diminished with age and is associated with immune checkpoint blockade efficacy in triple-negative breast cancer. Cancer Discov. 2019;9:1208–27.
72. Blank CU, Reijers ILM, Versluis JM, Menzies AM, Dimitriadis P, Wouters MW, et al. LBA39 Personalized combination of neoadjuvant domatinostat, nivolumab (NIVO) and ipilimumab (IPI) in stage IIIB-D melanoma patients (pts) stratified according to the interferon-gamma signature (IFN-γ sign): The DONIMI study. Ann Oncol. 2021;32:S1315.
73. Lin SH, Cheng PC, Tu S Te, Hsu SR, Cheng YC, Liu YH. Effect of metformin monotherapy on serum lipid profile in statin-naïve individuals with newly diagnosed type 2 diabetes mellitus: A cohort study. PeerJ [Internet]. 2018 [cited 2025 May 21];2018:e4578. Available from: https://pmc.ncbi.nlm.nih.gov/articles/PMC5899882/

FIGURE LEGENDS

Figure 1. Identification of c-kit as a cancer stem cell marker in fibrosarcoma MN/MCA-1. A-B) MN/MCA-1 cells were cultured under adherent conditions or spheroid-forming conditions. **A)** Representative images are shown. Scale bars 200μm. **B)** (left) Flow cytometry analysis of c-kit expression performed after 2 weeks of culture (n=6 for each condition); (right) mRNA expression levels (RT-PCR) of stemness-associated genes analyzed after 2 weeks of culture, *c-kit* (n=4 per condition; one experiment was performed), *Nanog* (shown are pooled data from n=2 experiments with n=3 samples for each condition), *Sox2* and *Oct4* (n=3 per condition; one experiment was

Downloaded from aacrjournals.org/cancerimmunolres/article-pdf/doi/10.1158/2326-6066.CIR-26-0211/3849116/cir-26-0211.pdf by guest on 22 November 2026

performed). **C)** Tumorigenic potential of FACS-sorted c-kit^{+} and c-kit^{-} MN/MCA-1 cells isolated from in vitro-grown spheroids following s.c. injection into WT C57BL/6 mice. The table on the right summarizes the results of n=2 in vivo independent experiments; **D)** Expression of c-kit and stemness-associated genes in MN/MCA-1 c-kit^{+} and c-kit^{-} cells, FACS-sorted from in vitro-grown spheroids (n=3 for each condition). **E)** (left) Experimental design: MN/MCA-1 fibrosarcoma cells were injected intramuscularly into WT C57Bl/6 mice and after 21 days, tumor infiltrating c-kit^{+} and c-kit^{-} cells were FACS-sorted; (middle) expression analysis of stemness-associated genes in c-kit^{+} and c-kit^{-} MN/MCA-1 cells (n=3 for each condition); (right) *ex vivo* spheroid-forming ratio of c-kit^{+} and c-kit^{-} MN/MCA-1 cells (n=5 for each condition). Data are presented as mean ± SEM. In B, D, E groups were compared by unpaired two-tailed T-test. *p<0.05, **p<0.005, ***p<0.001, ****p<0.0001 between selected relevant comparisons.

Figure 2. Loss of p50 NF-κB in the hematopoietic compartment is associated with reduced CSC frequency. **A**) Tumor growth of MN/MCA-1 fibrosarcoma in WT (n=5) and p50$^{-/-}$ (n=6) mice. **B**) (left) *Ex vivo* flow cytometry percentage of c-kit^{+}CD45^{-} cells in tumors isolated from WT and p50$^{-/-}$ mice (n=4); (right) mRNA expression analysis of stemness-associated genes by RT-PCR in c-kit^{+}CD45^{-} cells in tumors isolated from WT (n=4) and p50$^{-/-}$ (n=4) mice. **C**) Representative images of spheres obtained from *ex vivo* isolated cells from tumors grown in WT or p50KO (p50$^{-/-}$) mice and spheroid diameter. Scale bar 200μm. (WT, n=30; p50$^{-/-}$, n=16). **D**) RT-PCR analysis of EMT-associated markers in c-kit^{+} cells from tumors grown in WT (n=3) or p50$^{-/-}$ (n=3) mice. **E**) (left) Numbers of macroscopic lung metastases in WT and p50$^{-/-}$ mice (n=6); (right) percentage of c-kit^{+}mCherry^{+}CD45^{-} cells in the lungs of WT or p50$^{-/-}$ tumor-bearing mice (n=4 and 5, respectively). **F**) (left) Expression analysis of M1/M2 selected genes by RT-PCR in TAMs FACS-sorted from p50$^{fl/fl}$ (n=3) and p50$^{fl/fl}$*Tie2-Cre* MN/MCA1-bearing mice (n=3); (right) flow cytometry analysis of Tbet (T-box expressed in T cells) and GATA-3 (GATA binding protein 3) expression in tumor-infiltrating CD4^{+} T cells (n=3). **G**) (left) Percentage of c-kit^{+} cells in tumors

Downloaded from aacrjournals.org/cancerimmunolres/article-pdf/doi/10.1158/2326-6066.CIR-26-0211/3849116/cir-26-0211.pdf by guest on 22 November 2026

grown in $p50^{fl/fl}$ (n=4) vs $p50^{fl/fl}$*Tie2-Cre* (n=4) mice; (right) Expression analysis of stemness-associated genes by RT-PCR in tumors harvested from the same mice (shown are pooled data from n=2 experiments with respectively n=5 and n=6 samples for each condition). **H**) (left) Representative images of spheres obtained from tumor cells isolated from $p50^{fl/fl}$ and $p50^{fl/fl}$*Tie2-Cre* mice and maintained *in vitro* under spheroid-forming culture condition for 2 weeks. Scale bar 200μm; (right) histogram showing spheroid diameters. $p50^{fl/fl}$, n=54; $p50^{fl/fl}$*Tie2-Cre*, n=58. **I**) *Ex vivo* flow cytometry analysis of EMT-associated markers in c-$kit^{+}CD45^{-}$ cells in tumors grown in $p50^{fl/fl}$ (n=3) and $p50^{fl/fl}$*Tie2-Cre* (n=3) mice. **J**) Tumor growth kinetics of MN/MCA-1 fibrosarcoma cells injected into $p50^{fl/fl}$ (n=5) and $p50^{fl/fl}$*Tie2-Cre* (n=5) mice. **K**) (left) Numbers of lung metastases in $p50^{fl/fl}$ (n=11) and $p50^{fl/fl}$*Tie2-Cre* (n=10) MN/MCA-1-bearing mice; (middle) quantification of the area of metastatic burden from H&E-stained lung sections from the same samples; (right) percentage of total lung surface area occupied by metastases (n=4). Representative images are shown. Scale bars, 1 mm. All the data are expressed as mean ± SEM. Data are representative of two independent experiments. In A, J two-way ANOVA, in B, C, D, E, F, G, I, K (left) unpaired two-tailed T test, in H, K (right) Mann–Whitney U-test. *$p<0.05$, **$p<0.005$, ***$p<0.001$, ****$p<0.0001$ between selected relevant comparisons.

Figure 3. Loss of p50 NF-κB in tumor-infiltrating myeloid cells restrains cancer cell stemness and migratory capacity while remodeling the immune landscape of primary fibrosarcoma (MN/MCA-1). A-D) MN/MCA-1 cells were cultured in the presence of TSN obtained from tumors grown in $p50^{fl/fl}$ or $p50^{fl/fl}$*Tie2-Cre* mice. Data shown are representative of two independent experiments. **A**) (left) Representative images of spheroids obtained after 2 weeks of culture of tumor cells in the presence of TSN from $p50^{fl/fl}$ or $p50^{fl/fl}$*Tie2-Cre* mice. Scale bar 200 μm. (right) histogram shows the diameters of the spheroids. $p50^{fl/fl}$ (n=40) and $p50^{fl/fl}$*Tie2-Cre* (n=25). **B**) (left) Flow cytometric analysis of c-kit expression (n=8 or 6, respectively for $p50^{fl/fl}$ and $p50^{fl/fl}$*Tie2-Cre*)

Downloaded from aacrjournals.org/cancerimmunolres/article-pdf/doi/10.1158/2326-6066.CIR-26-0211/3849116/cir-26-0211.pdf by guest on 22 November 2026

(shown are pooled data from n=2 experiments with respectively n=4 $p50^{fl/fl}$ and n=3 $p50^{fl/fl}$*Tie2-Cre* mice) and (right) mRNA expression levels (qRT-PCR) of stemness-associated genes in MN/MCA-1 cells after 48 h of exposure to different TSNs (n=3 TSN $p50^{fl/fl}$ and n=4 TSN $p50^{fl/fl}$*Tie2-Cre*). **C**) Flow cytometric analysis of E-cadherin (left) and qRT-PCR analysis of N-cadherin (Cdh2) and vimentin (right) in c-kit$^+$ cells after 48 h of exposure of MN/MCA-1 cells to different TSNs (n=3). **D**) Scratch assay performed on MN/MCA-1 cells cultured in the presence of TSNs from $p50^{fl/fl}$ (n=3) and $p50^{fl/fl}$*Tie2-Cre* mice (n=3). Images of the recovered scratch area were acquired at T0 and after 48 h. Scale bar 1000 μm. On the right, histogram with the mean ± SEM distance between the two sides of the scratch, quantified using Image Analyzer software. **E-K**) MN/MCA-1 cells were injected intramuscularly (i.m.) into $p50^{fl/fl}$ and $p50^{fl/fl}$*Tie2-Cre* mice. After 22 days mice were sacrificed, and primary tumors were analyzed by FACS. $p50^{fl/fl}$ (n=13) and $p50^{fl/fl}$*Tie2-Cre* (n=8). Data are presented as mean ± SEM of 3 pooled independent experiments. **E**) t-SNE analysis of myeloid cells gated on CD45$^+$CD11b$^+$ cells after exclusion of dead cells. The dot plots show the distribution of the indicated immune cell populations. **F**) t-SNE analysis of tumor-infiltrating lymphoid cells. The dot plots show the distribution of the indicated immune cell populations. **G**) Frequencies of TAMs (CD11b$^+$F4/80$^+$), monocytes (CD11b$^+$Ly6C^{hi}) and dendritic cells (CD11c$^+$MHCII$^+$). **H**) (left) iNOS and TNFα (middle) expression in CD11b$^+$Ly6C^{hi} cells; (right) in vitro suppression assay assessing the ability of CD11b$^+$Ly6C^{hi} cells to inhibit splenic T cell proliferation at different MDSC-to-splenocyte ratios (25% and 50%). **I**) Frequencies of CD4$^+$, CD8$^+$ T cells, NK (CD3$^-$NK1.1$^+$) and NKT (CD3$^+$NK1.1$^+$). **J**) (left) IFNγ production, expressed as percentage of positive cells and mean fluorescence intensity (MFI), by tumor-infiltrating CD4$^+$ and CD8$^+$ cells; (right) GrzB expression by tumor infiltrating CD8$^+$ cells (n=8). **K**) qRT-PCR analysis of Th1-associated genes in CD4$^+$ T cells isolated from the spleen of $p50^{fl/fl}$ (n=3) and $p50^{fl/fl}$*Tie2-Cre* (n=4) tumor-bearing mice (n=3 and 4, respectively). Data are expressed as mean ± SEM. Unpaired two-tailed t-tests were used in A, B, G, H, I, and J; Mann–Whitney U-tests in C and K;

Downloaded from aacrjournals.org/cancerimmunolres/article-pdf/doi/10.1158/2326-6066.CIR-26-0211/3849116/cir-26-0211.pdf by guest on 22 November 2026

and two-way ANOVA in D. *p<0.05, **p<0.005, ***p<0.001, ****p<0.0001 between selected relevant comparisons.

Figure 4. Th1-polarized CD4$^+$ T cells limit cancer stemness and highlight the clinical relevance of Th1/Th2 immune polarization in sarcoma patients. A-B) CD4$^+$ cells were isolated from the spleens or the tumors of p50$^{fl/fl}$ (n=4) and p50$^{fl/fl}$*Tie2-Cre* (n=4) mice, injected i.m. with MN/MCA-1 cells, and co-cultured *in vitro* at a 3:1 ratio with MN/MCA-1 cells. After 48 h MN/MCA-1 cells were collected and plated in spheroid-forming conditions for 2 weeks. **A**) (left) Flow cytometry analysis of c-kit expression, among CD45$^-$ cells, after 48h of co-culture with splenic CD4$^+$ T cells from either p50$^{fl/fl}$ (n=4) or p50$^{fl/fl}$*Tie2-Cre* (n=4) mice; (right) number of spheroids obtained with MN/MCA-1 cells maintained in spheroid-forming conditions for one week (n=12 for splenic CD4 from p50$^{fl/fl}$ mice and n=5 for splenic CD4$^+$ cells from p50$^{fl/fl}$*Tie2-Cre* mice). **B**) (left) Flow cytometry analysis of c-kit expression, among CD45^{neg} cells, after 48h of co-culture with tumor-infiltrating CD4$^+$ T cells, obtained from either p50$^{fl/fl}$ (n=4) or p50$^{fl/fl}$*Tie2-Cre* (n=4) tumor-bearing mice; (right) number of spheroids obtained with MN/MCA-1 cells after one week of culture in spheroid-forming conditions (n=10 for tumor CD4 from p50$^{fl/fl}$ mice and n=8 for tumor CD4$^+$ cells from p50$^{fl/fl}$*Tie2-Cre* mice).. **C**) (left) representative images of spheroids from MN/MCA-1 cells maintained *in vitro* for 48 h in the absence (untreated, UNT) or in the presence of CD4$^+$ cells polarized *in vitro* towards Th0, Th1 or Th2 and then maintained under spheroid-forming conditions for 1 week. Scale bar 200 μm. (right) diagram with the diameters (n=100 spheroids per group) of the obtained spheroids. **D-G)** MN/MCA-1 cells injected i.m. into p50$^{fl/fl}$ and p50$^{fl/fl}$*Tie2-Cre* mice receiving anti-CD4 antibody (or vehicle as control) (n=5 mice for each experimental group). Data are representative of two independent experiments. **D**) Growth kinetics and **E)** number of lung metastases recorded at sacrifice) (n=4); **F**) Flow cytometric analysis of the percentage of c-kit$^+$ cells within the isolated tumors. **G**) Flow cytometry quantification of E-cadherin and Vimentin expression by tumor cells (n=3). **H**) MN/MCA-1 cells were maintained for one week under

Downloaded from aacrjournals.org/cancerimmunolres/article-pdf/doi/10.1158/2326-6066.CIR-26-0211/3849116/cir-26-0211.pdf by guest on 22 November 2026

spheroid-culture conditions in the presence of IFNγ (20 ng/ml) or IL-4 (20 ng/ml), or were left untreated (medium). (left) Representative images (scale bars 50 μm) and diagram with the diameters (n=70 spheroids per group) of the obtained spheroids; (center) flow cytometry quantification of c-kit^{+} CSC and (right) qRT-PCR analysis of EMT-related genes expression (n=3). **I**) MN/MCA-1 cells were cultured in the TSN obtained from tumors grown in p50$^{fl/fl}$ and p50$^{fl/fl}$*Tie2-Cre* mice, in the presence of either anti-IL-4 or anti-IFNγ antibodies (n=2 independent experiments). After 48h c-kit expression was evaluated by flow cytometry. Data are expressed as mean ± SEM; in A-B Mann–Whitney U-test, in D one-way ANOVA, in C-E-F-G-I-H two-way ANOVA, in H (left) Kruskal-Wallis test ANOVA *p<0.05, **p<0.005, ***p<0.001, ****p<0.0001 between selected relevant comparisons. **J)** Analysis of TCGA Kaplan–Meier survival curves of sarcoma patients stratified into high- and low-risk groups based on the median risk score. The risk score was derived from a Cox proportional hazards model for overall survival, using the genes of the Th1 signature as predictors. Differences in survival between groups were assessed using the log-rank test. **K)** Kaplan–Meier survival curves of sarcoma patients stratified according to the IFNγ expression levels. **L)** Violin plots depict serum levels of selected Th-1 polarizing cytokines in healthy donors (HD; n=20), sarcoma patients with no evidence of disease after surgery (NED; n=26) and sarcoma patients dead or alive with evidence of disease after surgery (AWD; n=18), with a mean time window for recurrence assessment of one year. Statistical significance of differences between patient groups was calculated using the Kruskal-Wallis test ANOVA *p<0.05, **p<0.005, ***p<0.001, ****p<0.0001. **M-N)** Boxplots of SOX2 and ZEB1 expression levels in sarcoma patients stratified by IFNγ expression status. Patients were classified into IFNγ-high and IFNγ-low groups based on the median IFNγ expression level. Statistical comparison of SOX2 and ZEB1 expression between groups was performed using Wilcoxon test. Boxplots show the median (central line), the first and third quartiles (bottom and top bounds of the box, respectively), and the minimum and maximum values (whiskers). Whisker length is limited to a maximum of 1.5 times the interquartile range (IQR), with data points falling outside this range plotted individually as

Downloaded from aacrjournals.org/cancerimmunolres/article-pdf/doi/10.1158/2326-6066.CIR-26-0211/3849116/cir-26-0211.pdf by guest on 22 November 2026

outliers. **O)** Scatterplot showing the association between Th1 signature and ZEB1 expression. The fitted linear regression line is displayed, and Spearman's rank correlation coefficient with the corresponding p-value is indicated

Figure 5. Relevance of Th1/Th2-dependent modulation of the CSC phenotype in DOXO resistance. A-D) MN/MCA-1 cells were maintained in spheroid-culture conditions in the presence of different concentrations of IFNγ (20 ng/ml and 0,2 ng/ml), IL-4 (20 ng/ml) or left untreated for 1 week, were treated or not with DOXO 0.7 μM. After 48h images were acquired and analysis were performed. **A**) Representative images (top) and quantification of spheroid diameters (bottom) in the different experimental groups. Scale bars 50 μM. (n=25 spheroids per group). **B**) Percentage of dead and live c-kit^{+} cells in the different experimental groups, treated or not with DOXO (n=3 for each experimental group). **C**) Flow cytometry analysis of spheroid cell viability through Annexin-PI assay (n=2). **D**) ABCG2 and MDR1 gene expression in spheroids in the different experimental groups (n=3). **E**) FACS quantification of intracellular DOXO in spheroids at the indicated time points (n=2). **F**) MN/MCA-1 cells were injected into p50$^{fl/fl}$ and p50$^{fl/fl}$*Tie2-Cre* mice, which after 10 days were treated intravenously with DOXO (1 mg/kg) (n=5 for p50$^{fl/fl}$ and n=4 for p50$^{fl/fl}$*Tie2-Cre*) or vehicle (as control) (n=4 for p50$^{fl/fl}$ and n=4 for p50$^{fl/fl}$*Tie2-Cre*). After 25 days, mice were sacrificed, and the number of lung metastasis was counted. Data are representative of two independent experiments. All the data are expressed as mean ± SEM. Two-way ANOVA was used for A (right), B, C, D, E, and F; one-way ANOVA followed by Tukey's multiple-comparisons test was used for A (left).

Figure 6. High and low IFNγ doses differentially activate STAT1 and AKT pathways, altering spheroid growth and chemosensitivity. A) MN/MCA-1 cells were cultured under spheroid-forming conditions in the presence of IFNγ (20 ng/ml or 0.2 ng/ml) or left untreated for 1 week. Cells were then harvested and analyzed by FACS to assess the expression of pSTAT1, STAT1,

Downloaded from aacrjournals.org/cancerimmunolres/article-pdf/doi/10.1158/2326-6066.CIR-26-0211/3849116/cir-26-0211.pdf by guest on 22 November 2026

pAKT and AKT. Representative MFI histograms of pSTAT1, pAKT (top) and STAT1, AKT (bottom) expression in the different experimental conditions are shown (n=3 for each experimental group). Data are representative of n=3 independent experiments. **B**) MN/MCA-1 cells were plated under spheroid-forming conditions and treated with Ruxolitinib (RX, 1 μM) or PF-04691502 (PF, 1 μM) for 1h, followed by IFNγ treatment (20 ng/ml or 0,2 ng/ml). After 1 week, images were acquired and analyses were performed. Representative images of spheroids (left) and quantification of spheroid diameters (right) in the different experimental groups. Scale bars 50 μm. (n=30 spheroids per group). Data are representative of n=2 independent experiments. **C-D**) MN/MCA-1 cells were plated under spheroid-forming conditions and treated with RX (1 μM) or PF (1 μM) for 1h, followed by IFNγ (20 ng/ml or 0,2 ng/ml) treatment. After 1 week, they were treated or not with DOXO 1 μM. **(C)** After 48 h, quantification of spheroids diameters in the different experimental groups (n=25 spheroids for each experimental group). **(D)** Flow cytometric analysis of cell viability by Annexin-PI assay (n=3 samples for each experimental group) was performed. Data are representative of n=2 independent experiments. All the data are expressed as mean ± SEM *$p<0.05$, **$p<0.005$, ***$p<0.001$, ****$p<0.0001$ between selected relevant comparisons. Two-way ANOVA was used for A, C, and D; the Kruskal–Wallis test was used for B.

Figure 7. Role of Th1/Th2 balance in anticancer therapy resistance. (A-D) MN/MCA-1 cells were injected into WT mice randomly divided to receive αPD-1 alone (100μg/mouse) or in combination with αIFNγ (200μg/mouse). Mice receiving only vehicle were used as control. Data shown are representative of two independent experiments. A) Tumor growth curves (n=4 mice/group). B) Percentage of IFNγ$^+$ cells among CD4$^+$ and CD8$^+$ T cells in tumors harvested from untreated, αPD-1 or αPD-1/αIFNγ-treated mice (n=4 mice/group). C) Percentage of (left) c-kit$^+$ (shown are pooled data from n=2 experiments with n=4 samples for each condition) and (right) E-

Downloaded from aacrjournals.org/cancerimmunolres/article-pdf/doi/10.1158/2326-6066.CIR-26-0211/3849116/cir-26-0211.pdf by guest on 22 November 2026

cadherin^{+} cells (n=4 for each experimental group) among CSC in tumors harvested from the different cohorts of mice. D) Numbers of lung metastases recorded at sacrifice in untreated, αPD-1 or αPD-1/αIFNγ-treated mice (n=5 mice/group). E) (Top), MN/MCA-1 cells were injected into WT C57/Bl6 mice, randomly divided to receive αPD-1 (100μg/mouse), DOXO (1mg/kg), αIFNγ (200μg/mouse), alone or in co-treatments as indicated (n=5-6 mice/group). (bottom), MN/MCA-1 cells were injected into WT C57/Bl6 mice, randomly divided to receive DOXO (1mg/kg), IFNγ (1μg/mouse), αIFNγ (200μg/mouse), alone or in co-treatments as indicated (n=5-6 mice/group). Tumor volumes and numbers of lung metastases recorded at the sacrifice are reported. F) MN/MCA-1 cells were injected into WT C57/Bl6 mice, divided to receive decreasing doses of IFNγ (0.1, 0.01, or 0.001 μg/mouse), alone or in co-treatment with DOXO (1mg/kg) (n=5-6 mice/group). Vehicle-treated mice were used as controls. (left) Tumor volume (center) and numbers of lung metastases recorded at the sacrifice; (right) representative images of lungs in the different experimental groups are shown. G) MN/MCA-1 cells were injected into WT C57/Bl6 mice, randomly divided to receive αPD-1 (100μg/mouse), DOXO (1mg/kg), IFNγ (1μg/mouse), αIL-4 (200μg/mouse) alone or in co-treatments as indicated (n=5-6 mice/group). Tumor volume (left) and numbers of lung metastases (right) recorded at the sacrifice are reported. All the data are expressed as mean±SEM; *$p<0.05$, **$p<0.005$, ***$p<0.001$, ****$p<0.0001$ between selected relevant comparisons. In A two-way ANOVA with Šidák's multiple comparisons test, in B-C-D ordinary one-way ANOVA, in E-F-G Kruskal-Wallis test ANOVA.

Downloaded from aacrjournals.org/cancerimmunolres/article-pdf/doi/10.1158/2326-6066.CIR-26-0211/3849116/cir-26-0211.pdf by guest on 22 November 2026

Downloaded from aacrjournals.org/cancerimmunolres/article-pdf/doi/10.1158/2326-6066.CIR-26-0211/3849116/cir-26-0211.pdf by guest on 22 November 2026

FIGURE 1

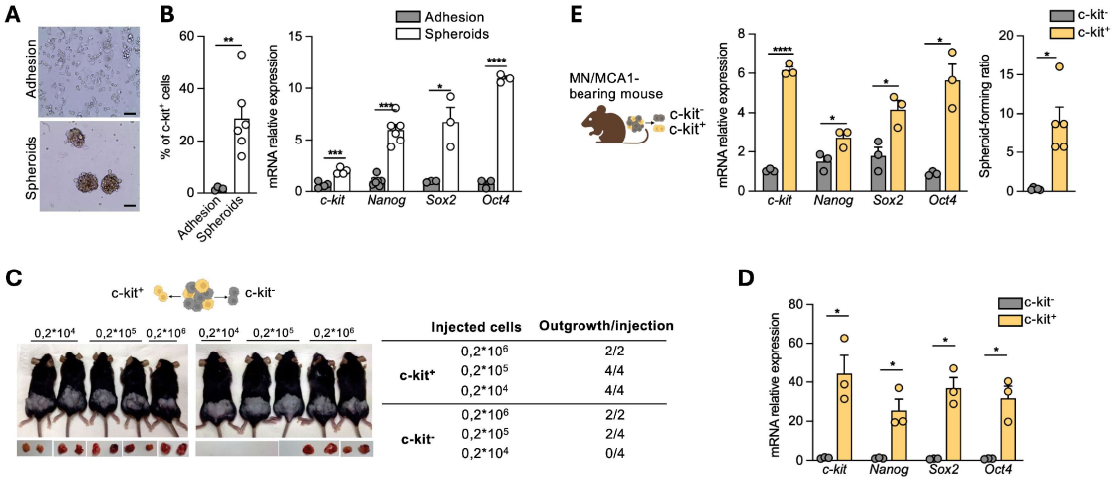

	Injected cells	Outgrowth/injection
c-kit+	0,2*10⁶	2/2
	0,2*10⁵	4/4
	0,2*10⁴	4/4
c-kit-	0,2*10⁶	2/2
	0,2*10⁵	2/4
	0,2*10⁴	0/4

FIGURE 2

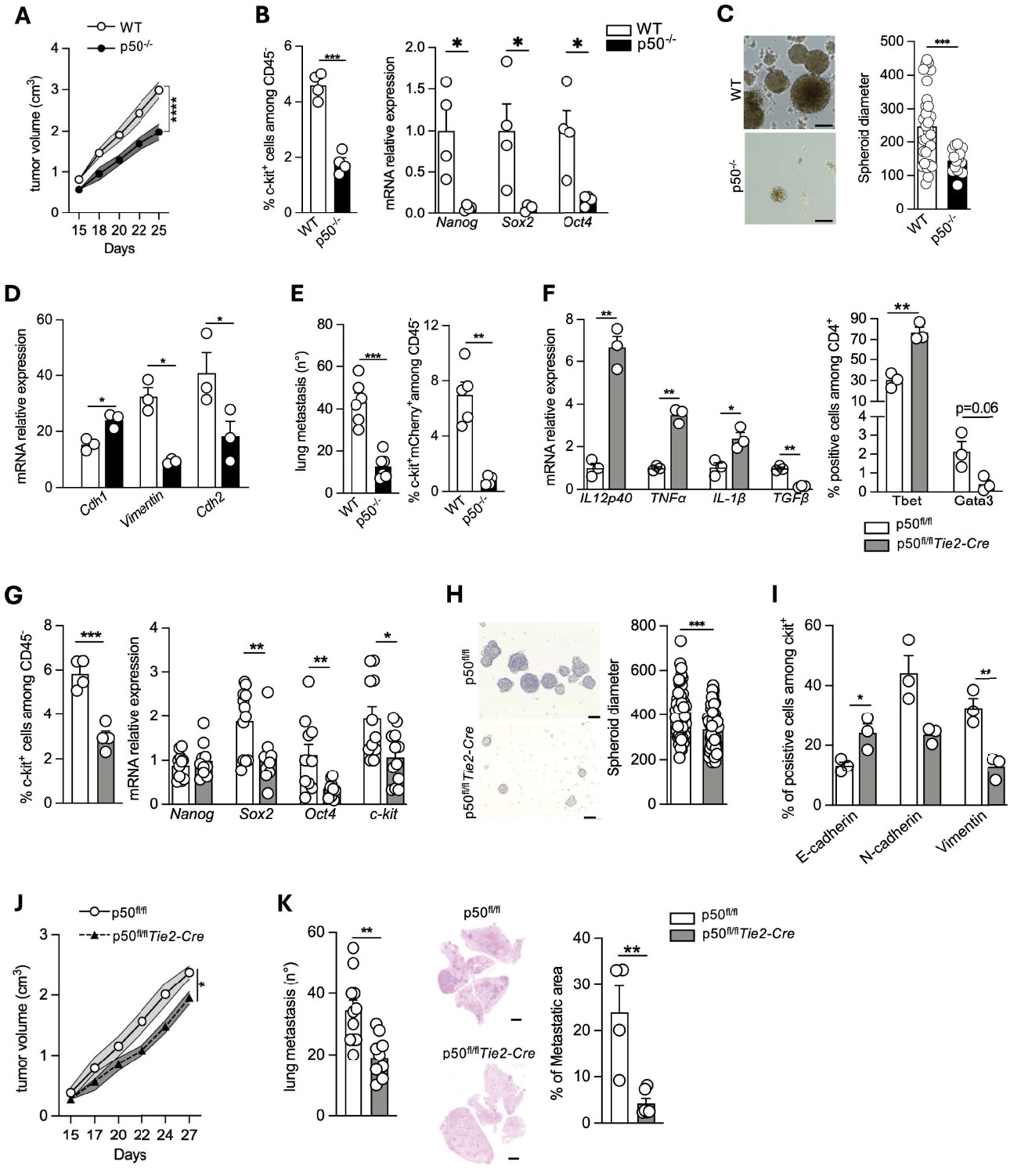

Downloaded from aacrjournals.org/cancerimmunolres/article-pdf/doi/10.1158/2326-6066.CIR-26-0211/3849116/cir-26-0211.pdf by guest on 22 November 2026

FIGURE 3

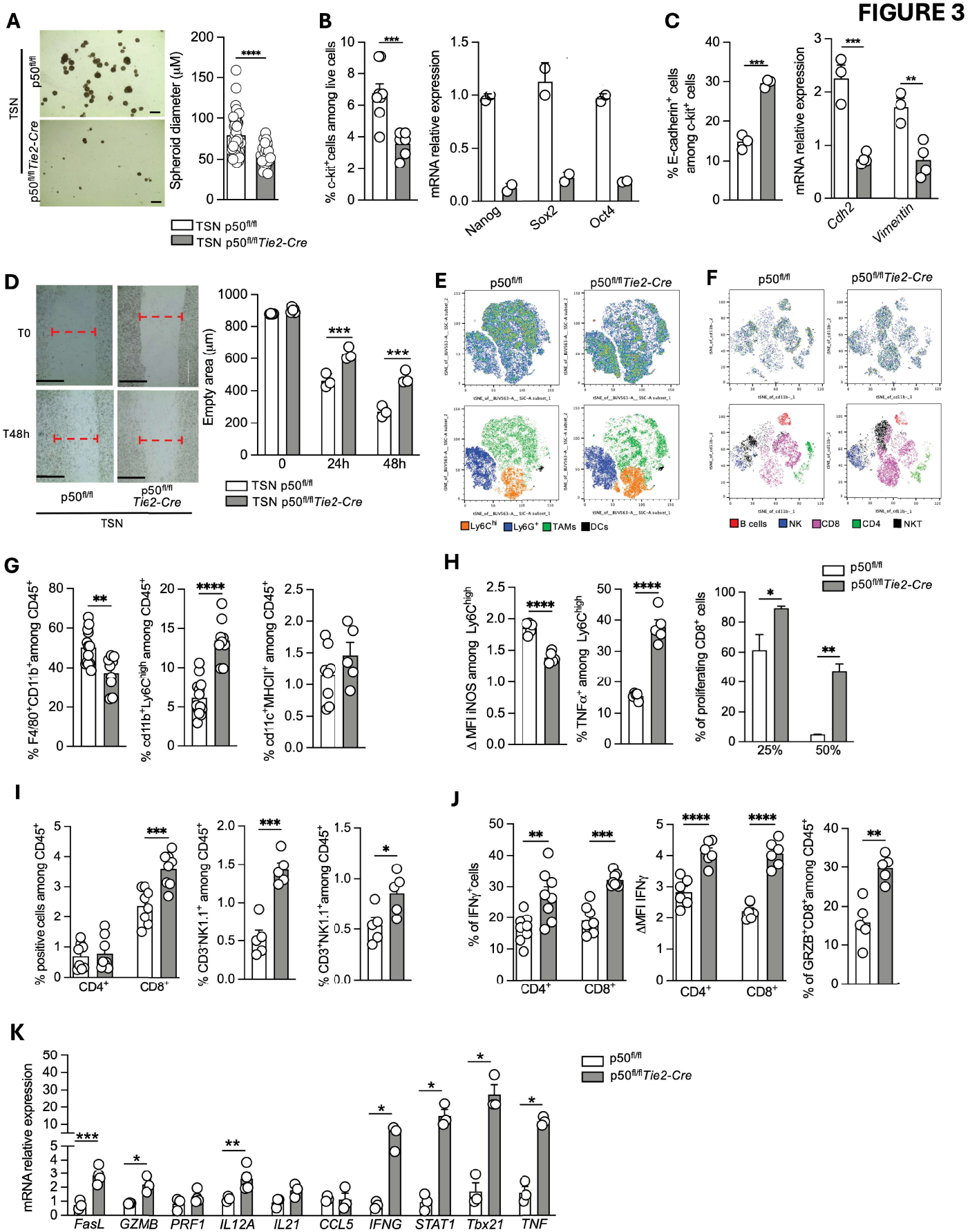

Downloaded from aacrjournals.org/cancerimmunolres/article-pdf/doi/10.1158/2326-6066.CIR-26-0211/3849116/cir-26-0211.pdf by guest on 22 November 2026

FIGURE 4

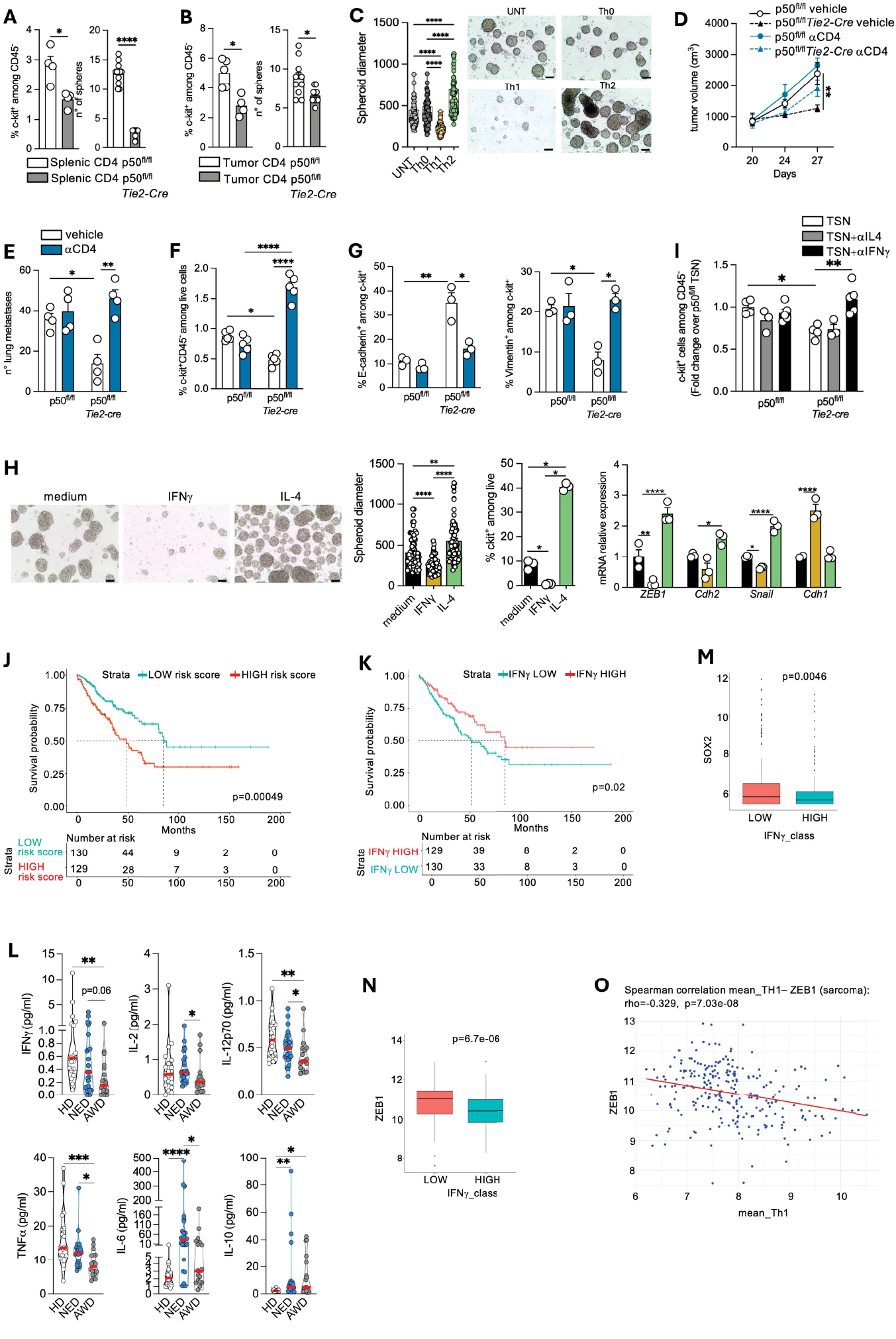

Downloaded from aacrjournals.org/cancerimmunolres/article-pdf/doi/10.1158/2326-6066.CIR-26-0211/3849116/cir-26-0211.pdf by guest on 22 November 2026

Downloaded from aacrjournals.org/cancerimmunolres/article-pdf/doi/10.1158/2326-6066.CIR-26-0211/3849116/cir-26-0211.pdf by guest on 22 November 2026

FIGURE 5

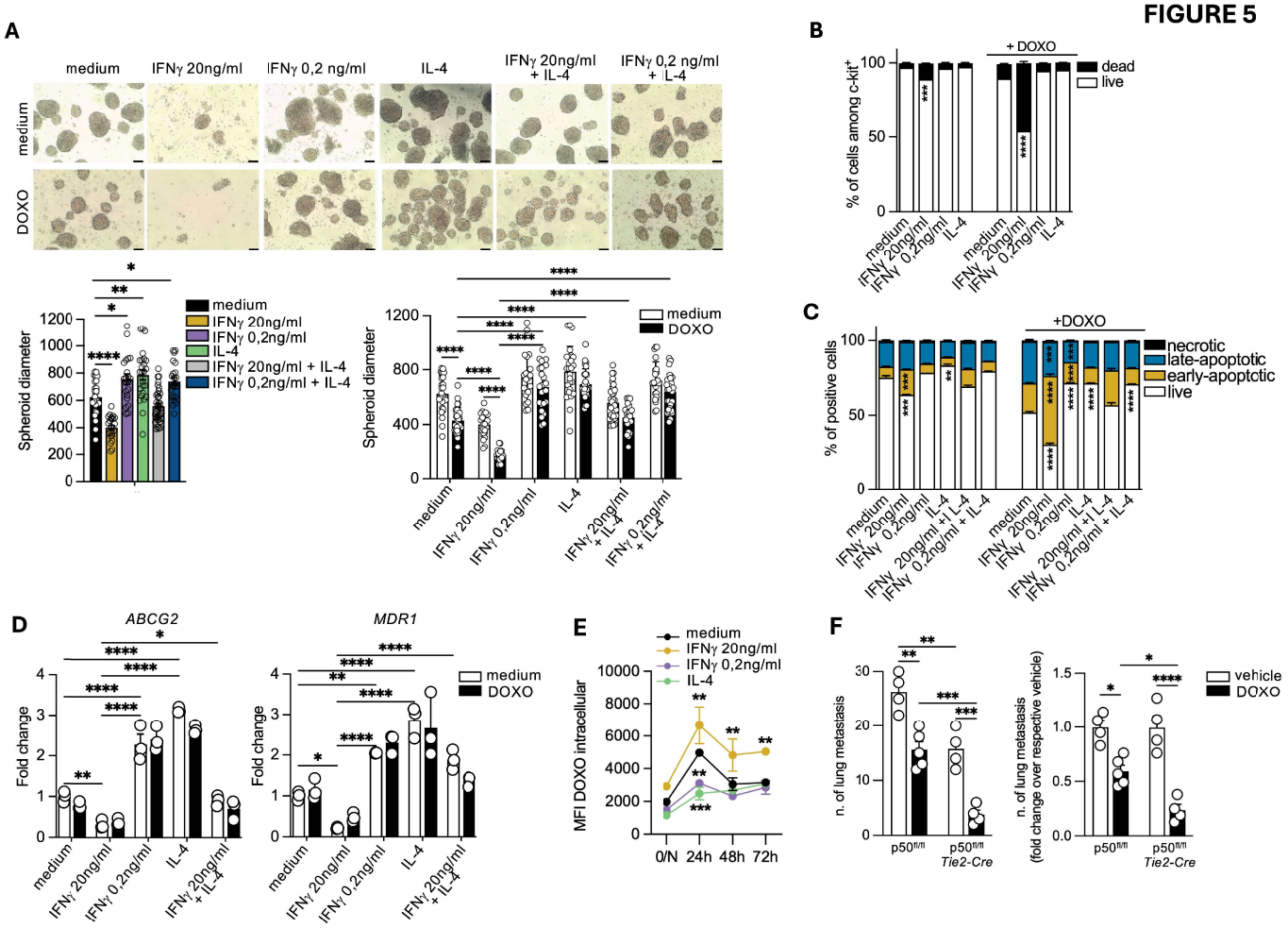

Downloaded from aacrjournals.org/cancerimmunolres/article-pdf/doi/10.1158/2326-6066.CIR-26-0211/3849116/cir-26-0211.pdf by guest on 22 November 2026

FIGURE 6

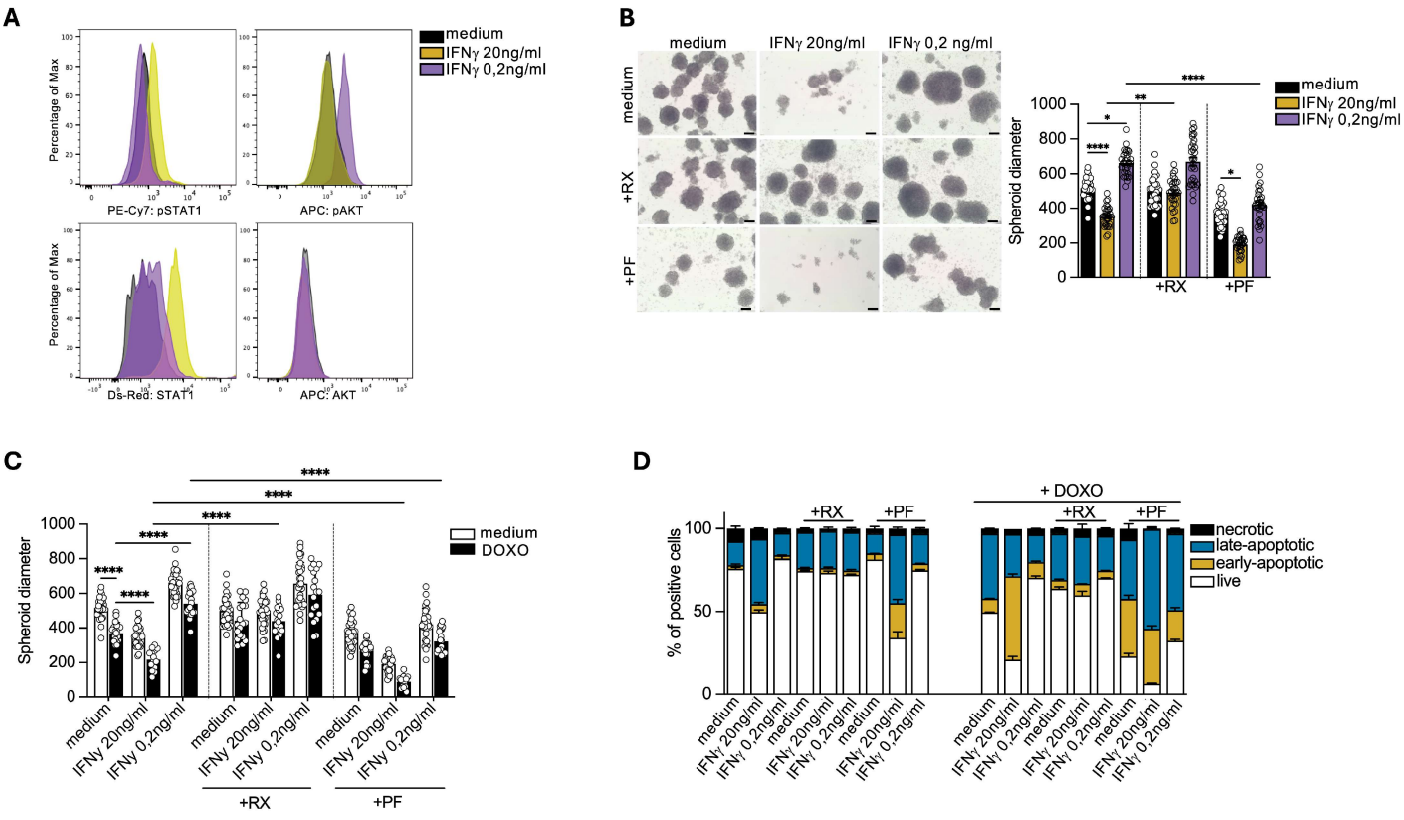

FIGURE 7

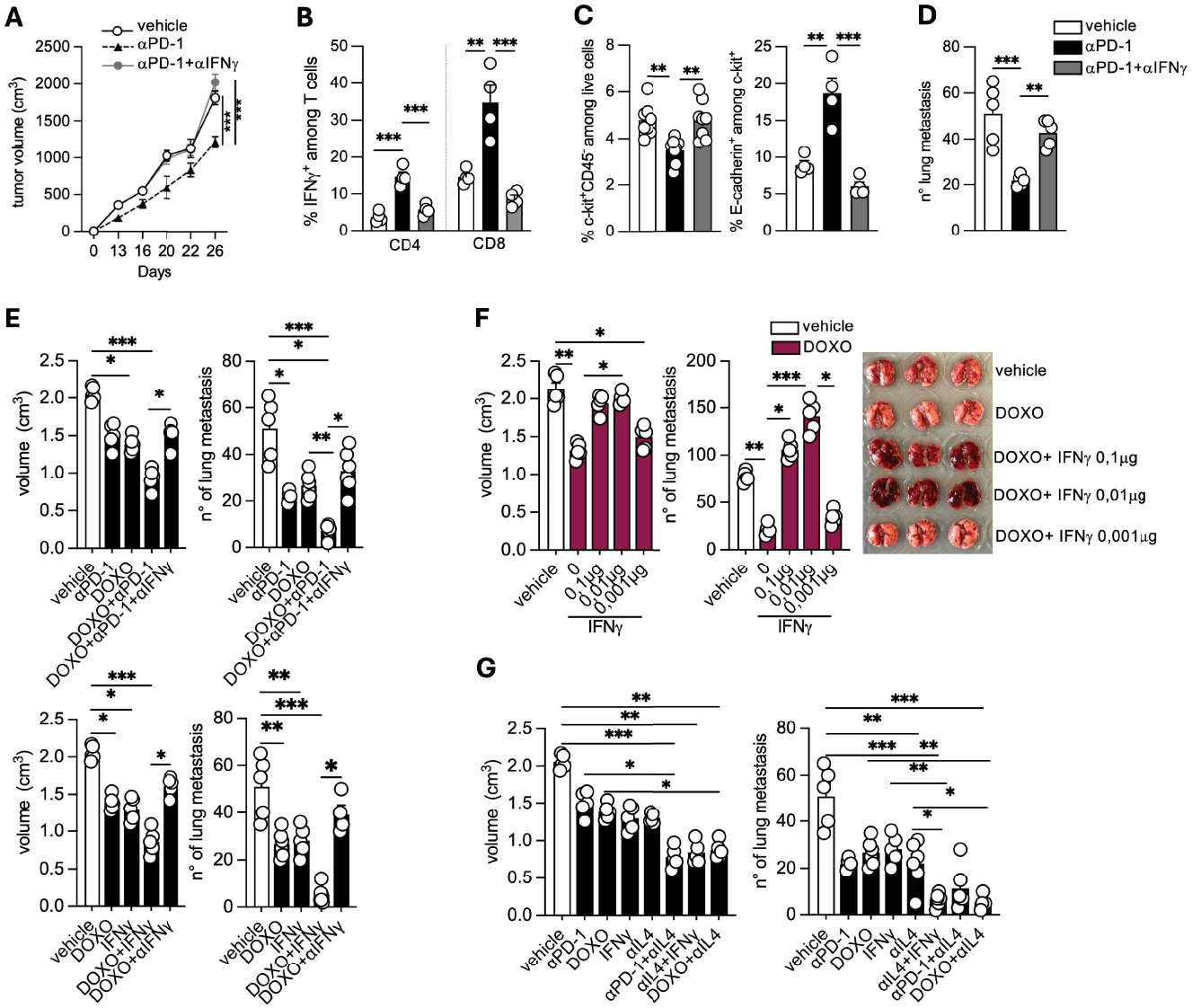

Downloaded from aacrjournals.org/cancerimmunolres/article-pdf/doi/10.1158/2326-6066.CIR-26-0211/3849116/cir-26-0211.pdf by guest on 22 November 2026